Precambrian Research 181 (2010) 43–63

Contents lists available at ScienceDirect

Precambrian Research

journal homepage: www.elsevier.com/locate/precamres

Regional and global chemostratigraphic correlation of the early Neoproterozoic Shaler Supergroup, Victoria Island, Northwestern Canada

D.S. Jones[a,*], A.C. Maloof[b], M.T. Hurtgen[c], R.H. Rainbird[d], D.P. Schrag[a]

[a] Department of Earth and Planetary Sciences, Harvard University, 20 Oxford Street, Cambridge, MA 02138, USA
[b] Department of Geosciences, Princeton University, 213 Guyot Hall, Princeton, NJ 08544, USA
[c] Department of Earth and Planetary Sciences, Northwestern University, 1850 Campus Drive, Evanston, IL 60208, USA
[d] Geological Survey of Canada, 601 Booth Street, Ottawa, ON, Canada K1A 0E8

ARTICLE INFO

Article history:
Received 15 October 2008
Received in revised form 14 April 2010
Accepted 5 May 2010

Keywords:
Shaler Supergroup
Neoproterozoic
Isotope stratigraphy
Chemostratigraphic correlation
Victoria Island
Mackenzie Mountains Supergroup

ABSTRACT

High resolution inorganic carbon isotope stratigraphy provides a new tool for correlating the Neoproterozoic Shaler Supergroup with the Mackenzie Mountains Supergroup. Previous stratigraphic studies established a widely accepted basis for correlation between the two supergroups. This contribution introduces a revised, testable hypothesis for the correlation of the Shaler and Mackenzie Mountains supergroups, based on matching distinctive features in the Shaler Supergroup $\delta^{13}C$ data with the previously published $\delta^{13}C$ curve for the Mackenzie Mountains Supergroup. The hypothesis suggests that some lithologically similar units in the two basins were deposited diachronously, and that a significant disconformity may exist within the Wynniatt Formation of the Shaler Supergroup. An important implication of the newly proposed correlation is that the flora and fauna of the Wynniatt Formation predate the "Bitter Springs" isotopic stage, placing a new constraint on the chronology of the Neoproterozoic fossil record.

1. Introduction

The early Neoproterozoic was the time of transition from the relative environmental quiescence of the Mesoproterozoic Era to the dramatic evolutionary, geochemical, and climatological events of the Cryogenian and Ediacaran periods (e.g., Anbar and Knoll, 2002; Bartley and Kah, 2004; Hoffman, 1999). The development of a better understanding of the history of this critical interval has been hindered by difficulties in the global correlation of the early Neoproterozoic sedimentary record. In the absence of biostratigraphically useful index fossils and high-precision U–Pb ages, advances in global Neoproterozoic stratigraphic correlation have relied largely on (a) detailed $\delta^{13}C$ chemostratigraphy (e.g., Kaufman and Knoll, 1995; Hill and Walter, 2000; Halverson et al., 2005), and (b) lithostratigraphic correlation based on the global occurrence of diagnostic sedimentary structures in the cap carbonates of Cryogenian glacial deposits (e.g., Allen and Hoffman, 2005).

This contribution presents new high-resolution $\delta^{13}C$ data from the Shaler Supergroup on Victoria Island in northwestern Canada (Fig. 1). These chemostratigraphic data are then used to propose regional and global correlations with other Neoproterozoic sedimentary successions. Lithostratigraphic observations have long been used to correlate the Shaler Supergroup with the Mackenzie Mountains Supergroup, also in northwest Canada (Fig. 2). In Neoproterozoic time the two regions were part of the same superbasin in northwest Laurentia. The $\delta^{13}C$ curve from the Shaler Supergroup is compared with a published $\delta^{13}C$ record from the Mackenzie Mountains Supergroup (Halverson, 2006). The new data have several trends and features recognizable in the data from Mackenzie Mountains Supergroup. While some of these features occur in strata that are traditionally thought to be correlative based on lithostratigraphy, others occur in lithostratigraphically distinct units. On the basis of these observations a new hypothesis regarding the correlation of the Shaler and Mackenzie Mountains supergroups is developed, emphasizing the observation that similar lithofacies are not always time-equivalents.

The new geochemical dataset provides a means of integrating the Shaler Supergroup into the global picture of the evolving Neoproterozoic Earth. Such a synthesis is critical for placing the diverse Shaler fauna and flora (Butterfield and Rainbird, 1998; Butterfield, 2005a,b) into the complex history of instability and change in Neoproterozoic carbon cycling, climate, and geodynamics. The Shaler Supergroup hosts acritarchs and multicellular eukaryotes, and it may contain stem-group dinoflagellates (Butterfield and Rainbird, 1998). The correlation hypothesis presented here implies that the Shaler Supergroup fauna predates the "Bitter Springs Stage" (BSS)

* Corresponding author. Current address: Department of Earth and Planetary Sciences, Washington University in St. Louis, 1 Brookings Drive, St. Louis, MO 63130, USA. Tel.: +1 718 506 7045; fax: +1 314 935 7361.
E-mail address: djones@levee.wustl.edu (D.S. Jones).

0301-9268/$ – see front matter © 2010 Elsevier B.V. All rights reserved.
doi:10.1016/j.precamres.2010.05.012

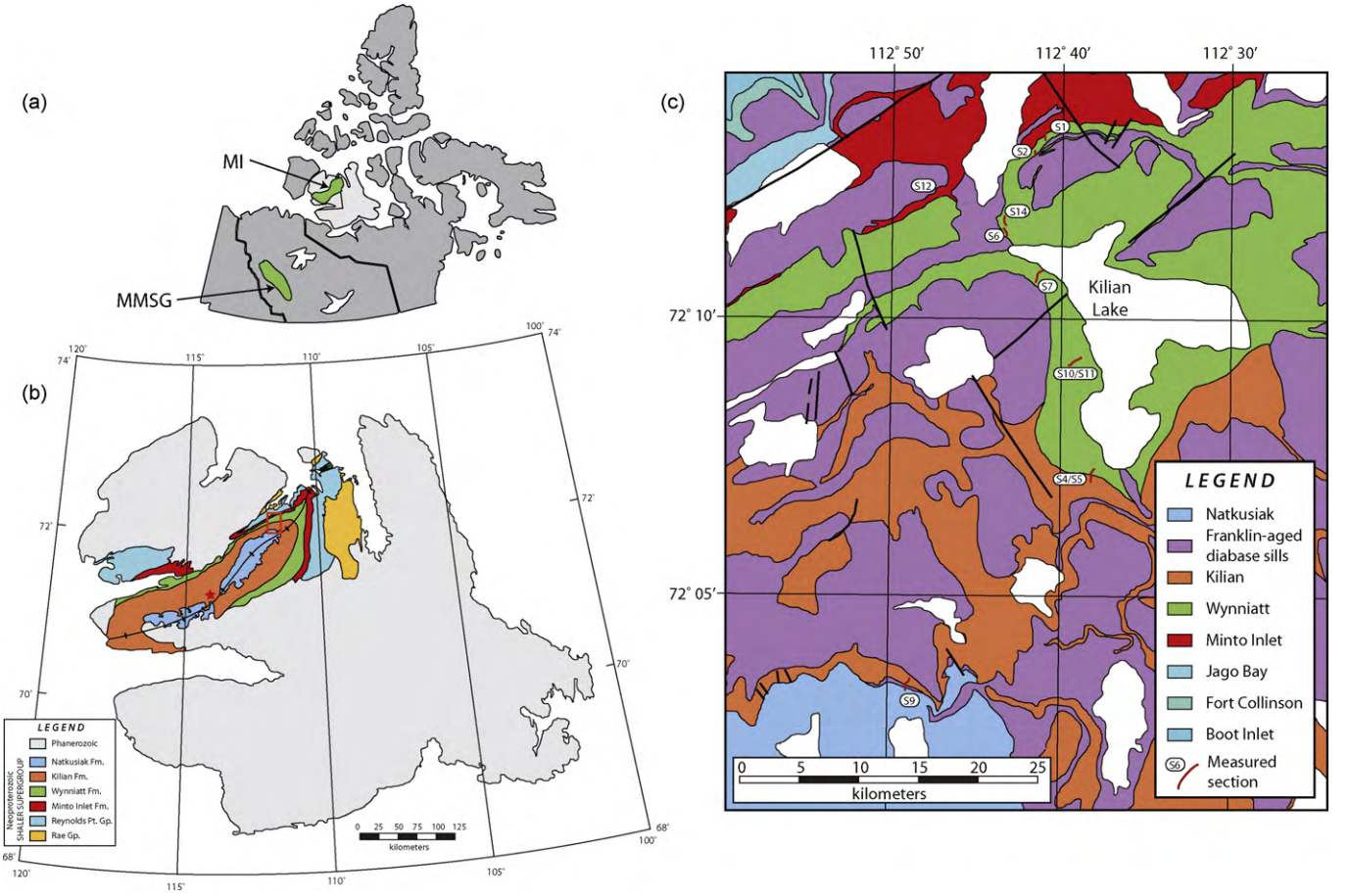

Fig. 1. Geologic maps of the study area: (a) location of Minto Inlier (MI) and Mackenzie Mountains Supergroup (MMSG); (b) formations of the Proterozoic Minto Inlier, modified from Christie et al. (1963); (c) northeastern domain of Minto Inlier, modified from Rainbird et al. (1995). Red star in panel (b) indicates location of section 05RAT53. Red box in panel (b) marks area expanded in panel (c). (For interpretation of the references to color in this figure legend, the reader is referred to the web version of the article.)

of the early Neoproterozoic. The BSS is the first large negative $\delta^{13}C$ excursion of the Neoproterozoic (Halverson et al., 2007b) and is thought to mark an episode of true polar wander (TPW) (Maloof et al., 2006). Any phylogenetic inference made from the Wynniatt Formation fossils will benefit from the resolution of the chronostratigraphic issue the new $\delta^{13}C$ stratigraphy present.

2. Geologic setting

Victoria Island is located in the Canadian Arctic Archipelago (Fig. 1). Neoproterozoic sedimentary and volcanic rocks of the Shaler Supergroup are exposed in the Minto Inlier, a ~350 km long and 100 km wide northeast–southwest trending topographic high that runs across the island (Thorsteinsson and Tozer, 1962). These rocks were deposited in the Amundsen Basin (Amundsen Embayment of Young (1981)), a shallow cratonic sea on northwestern (present coordinates) Laurentia within the supercontinent Rodinia (Rainbird et al., 1996). The primary structure of the Minto Inlier is the Holman Island Syncline, which produces gentle dips (generally $< 10^{\circ}$) on both limbs (Christie et al., 1963).

2.1. Stratigraphy

Northwestern Laurentia contains an extensive Proterozoic stratigraphic record. Three unconformity-bounded sedimentary successions are recognized; from oldest to youngest they are referred to as Successions A, B, and C (Young et al., 1979). The Shaler Supergroup is part of Succession B, as is the Mackenzie Mountains Supergroup of the northern Cordillera. Other putative Succession B strata include the Katakturuk Dolomite (Sadelerochit-Shublik Mountains), the Lower Tindir Group (Tatonduk Inlier), Fifteen Mile Group (Coal Creek and Hart River Inliers), and the Pinguicula Group (Wernecke Mountains) (Rainbird et al., 1996). However, recent stratigraphic and chemostratigraphic studies have challenged some of these traditional correlations; for example, the Katakturuk Dolomite has been shown to be younger (Macdonald et al., 2009b), and the Penguicula Group is significantly older (Thorkelson et al., 2005).

The Shaler Supergroup (Fig. 2) consists of, in ascending order, the Rae Group (Escape Rapids, Mikkelsen Islands, Nelson Head, and Aok formations), the Reynolds Point Group (Grassy Bay, Boot Inlet, Fort Collinson, and Jago Bay formations), and a set of ungrouped formations (Rainbird et al., 1996 and references within). The ungrouped formations are the Minto Inlet, Wynniatt, Kilian, and Kuujjua formations.

The *Rae Group* unconformably overlies Paleoproterozoic sedimentary rocks of the Goulburn Supergroup (Thorsteinsson and Tozer, 1962) along the northeastern margin of Minto Inlier (Campbell, 1981) and overlies Mesoproterozoic sedimentary rock of the Husky Creek Formation in the Coppermine Homocline west of Coronation Gulf (Baragar and Donaldson, 1973). The Escape Rapids and Mikkelsen Islands formations represent a marine transgression and subsequent development of an intertidal-supratidal carbonate platform (Rainbird et al., 1994). The mudstones and

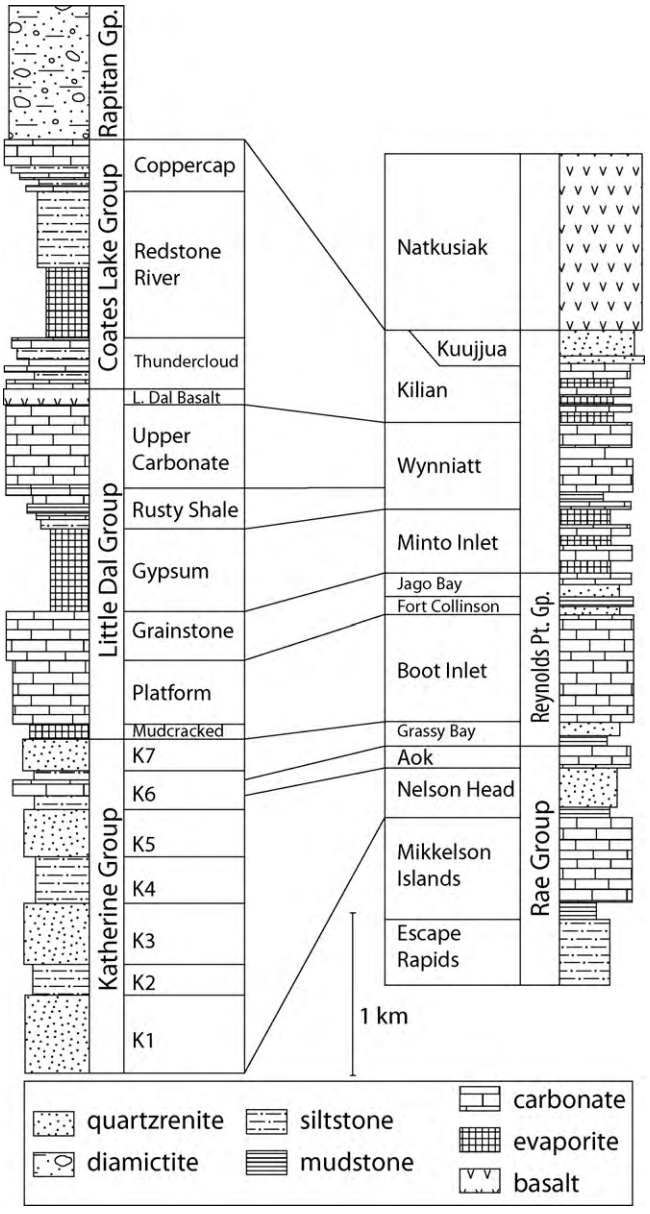

Fig. 2. Generalized stratigraphy of the Shaler Supergroup in the Minto Inlier, Victoria Island (Rainbird et al., 1994) and its lithologic correlation to the Mackenzie Mountains Supergroup, northwest Canada, redrawn from Rainbird et al. (1996).

quartzarenites of the Nelson Head Formation have been interpreted as a prograding marine delta overlain by a regionally extensive fluvial braidplain (Rainbird et al., 1994). The top of the Nelson Head Formation is marked by a major marine transgression with deposition of fine-grained siliciclastic rocks which are overlain by a distinctive orange-weathering stromatolitic dolostone, the Aok Formation (Fig. 3a) (Rainbird et al., 1994). This stromatolitic unit has traditionally been used as a marker bed throughout the Amundsen Basin and the Mackenzie Mountains (Jefferson and Young, 1989; Rainbird et al., 1996).

Above the Rae Group, the alternating clastic-dominated and carbonate-dominated formations of the *Reynolds Point Group* have been interpreted to represent third-order sequences corresponding to eustatic sea level changes on a subsiding platform (Morin and Rainbird, 1993). The lowermost unit, the Grassy Bay Formation, begins with a carbonaceous mudstone that represents drowning of the Aok carbonate platform. Young and Long (1977) attributed this facies change to an abrupt increase in subsidence rate. The deep water mudstone coarsens upward, representing a prograding delta. These pass to fluvial quartzarenites before clastic sediment supply ceased, allowing for the reestablishment of significant carbonate sedimentation (Young and Long, 1977). The overlying Boot Inlet Formation is interpreted to be a cyclically prograding, storm-dominated carbonate ramp; it includes a well-studied patch reef facies (Morin and Rainbird, 1993; Narbonne et al., 2000). Above the Boot Inlet Formation, the cross-bedded, carbonate-cemented, quartzarenites of the Fort Collinson Formation are thought to be fluvial deposits reworked in a shallow marine setting. These grade into intertidal to lagoonal carbonates of the Jago Bay Formation (Rainbird et al., 1994).

The formations above the Reynolds Point group are, from oldest to youngest, the Minto Inlet (Fig. 3b), Wynniatt (Fig. 3c), Kilian (Fig. 3d), Kuujjua, and Natkusiak (Fig. 3d) formations. The Minto Inlet Formation is comprised of <100 m to 250 m of interbedded sulfate evaporites and carbonates (Fig. 3b). It likely represents a period of high and fluctuating salinity due to intermittent closing of interior seaways connecting the intracratonic Amundsen Basin to the open ocean (Young, 1981). The base of the overlying Wynniatt Formation marks a return to shallow marine conditions with normal salinity (Fig. 3c). Dolostones of the Wynniatt Formation display textures characteristic of an energetic subtidal and intertidal zone, including mudcracks (Fig. 4a), ribbonites (i.e., dolosiltites deposited above storm wave base), ooids (Fig. 4b), intraformational conglomerate (Fig. 4c), and stromatolites. There are rare evaporitic beds in the Wynniatt Formation, indicating intermittent returns to the sabkha-like conditions of Minto Inlet time. The Kilian Formation conformably overlies the Wynniatt; it consists of two cycles of subtidal to supratidal relative sea level change (Rainbird, 1991, 1993). In the northeast domain of the Minto Inlier, six Kilian units are recognized: the lower evaporite member (Fig. 4d), the lower cyclic carbonate member, the middle evaporite member, the upper cyclic carbonate member, the clastic-carbonate member, and the tan carbonate member (Rainbird, 1991). In section S9, a series of peritidal parasequences ends abruptly with a previously undocumented flooding surface. Overlying the flooding surface is a siltstone overlain by a diamictite. The diamictite is 6–11 m thick with a violet argillite matrix, angular centimeter-sized dolostone clasts, and sand-sized stringers and grain trains. Above the diamictite are several meters of siltstone and limestone breccias, all indicative of deep water sedimentation. In the southwest domain, the flooding surface at the top of the Kilian Formation is not observed; rather the formation contains an upper evaporite member and a red shaly carbonate member above the tan carbonate member. In the southwest, carbonate sedimentation comes to an abrupt end at the Kilian-Kuujjua contact, where mature fluvial quartzarenites appear. The Kuujjua is interpreted to represent a wide braided river system with a southeasterly source.

A low angle unconformity separates the top of the Shaler Supergroup from the overlying Natkusiak Formation in the northeast domain (Jefferson, 1985). In the northeast domain, lahar-like volcaniclastic diamictite (Rainbird, 1993) fills decameter-scale grabens in the Kilian tan carbonate member (Fig. 3d). The dominant lithology of the Natkusiak is amygdaloidal basalt with vesicular, ferruginized flow tops. These basalts are derived from the same magmas that fed the numerous diabase sills that intrude the Shaler Supergroup throughout the Minto Inlier as demonstrated by field (Jefferson, 1985) and petrogenetic studies (Dostal et al., 1986). Further geochronology studies may be able to distinguish whether there were multiple episodes of sill emplacement.

2.2. Geochronology

There are few high-precision radiometric dates to constrain the age of the Shaler Supergroup. A minimum age of 723^{+4}_{-2} Ma is pro-

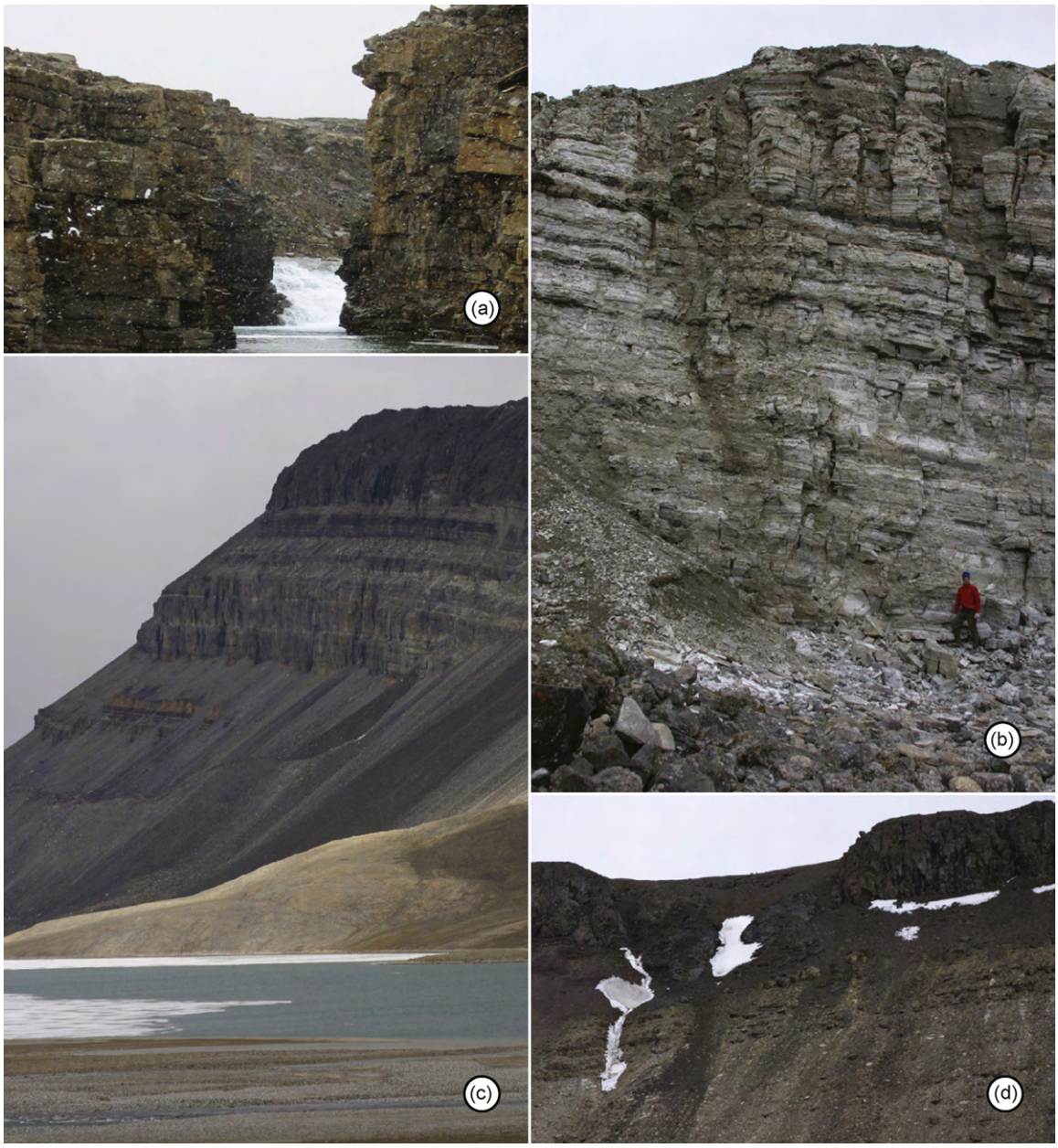

Fig. 3. Rocks of the Shaler Supergroup. (a) Aok Formation: orange-weathering grainstones and biostromes. Cliff on right is ~10 m tall. (b) Minto Inlet Formation: interbedded anhydrite and grey limestone ribbonite. (c) Wynniatt Formation: grey carbonates with dark resistant diabase sills at top. Sill is ~ 20 m thick. (d) Kilian and Natkusiak formations: block faulting dropping Natkusiak diamictite and basalt flows onto Kilian tan carbonate member. Photo shows ~70 m of strata. (For interpretation of the references to color in this figure legend, the reader is referred to the web version of the article.)

vided by a composite suite of U–Pb dates from baddeleyite and zircons from the numerous diabase sills that intrude the Minto Inlier (Heaman et al., 1992). The sampled material includes the uppermost sill below the Natkusiak flood basalts in the northeastern domain, where it intrudes the tan carbonate member of the Kilian Formation. The Natkusiak flood basalts capping the Shaler Supergroup have not been directly dated, but the uppermost sill intrudes the lowest basalt flow in the southwestern domain of the Minto Inlier (Heaman et al., 1992); therefore, the oldest flood basalts are no younger than 723 Ma.

A maximum age of 1267 ± 2 Ma for the base of the Shaler Supergroup is provided by a U–Pb (baddeleyite) age obtained from the Mackenzie Dike Swarm (LeCheminant and Heaman, 1989), which intrudes and feed the extensive basaltic flows of the Coppermine River Group (Baragar and Donaldson, 1973). The Coppermine Group is in turn unconformably overlain by the Rae Group, which is the lowermost stratigraphic package of the Shaler Supergroup on Victoria Island. Single grain analysis of detrital zircons (TIMS) from fluvial quartzarenites of the Nelson Head Formation yielded an age of 1077 ± 4 Ma (Rainbird et al., 1992), providing a maximum age for the upper Rae Group and for the chemostratigraphic data presented here, which are all derived from strata above the Nelson Head Formation.

Radiometric data therefore constrain deposition of the Reynolds Point Group and overlying strata between < 1077 and 72 Ma, a 350 Ma interval.

3. Chemostratigraphy

New high-resolution, stratigraphically controlled $\delta^{13}C$, and $\delta^{18}O$ measurements for carbonate rocks of the Shaler Supergroup are presented (Table 1). The analysis begins in the stromatolites of the

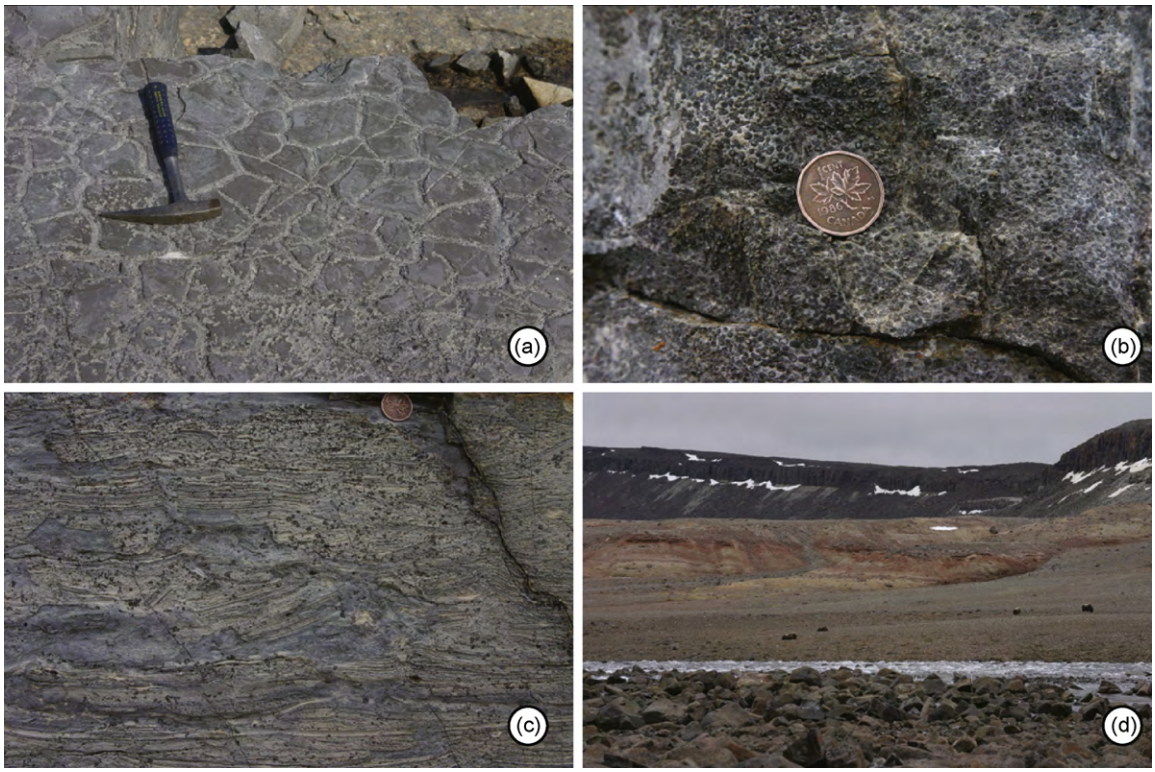

Fig. 4. Wynniatt Formation: (a) polygonal mudcrack surface in grey limestone ribbonite (section S6); (b) ooids in grey limestone grainstone (section S14); (c) intraformational conglomerate in grey limestone ribbonite (section S14). Kilian Formation: (d) bedded anhydrite, red and orange siltstone and argillite (section S4, muskoxen for scale). (For interpretation of the references to color in this figure legend, the reader is referred to the web version of the article.)

Aok Formation (Rae Group), and extend through the upper Kilian Formation. Samples were collected from the area near Kilian Lake, in the northeast part of the Minto Inlier (Fig. 1c, coordinates listed in Table 2). An additional small set of samples of the uppermost Kilian Formation was collected from one section in the southwest domain (section 05RAT53, Fig. 1b).

3.1. $\delta^{13}C$ and δ^{18} O methods

Carbonate samples were collected at regular intervals in the course of stratigraphic logging and geologic mapping. Clean limestones and dolostones with minimal siliciclastic component or secondary veining were sampled. Samples were slabbed, and 10–50 mg of powder were microdrilled from fresh surfaces along bedding where visible. Carbonate powders were baked in a 40 °C oven for at least 12 h to eliminate any residual water. $\delta^{13}C$ and δ^{18} O were measured simultaneously at the Harvard University Laboratory for Geochemical Oceanography on a VG Optima dual inlet mass spectrometer with a modified Isocarb preparation device. Approximately 1 mg of each sample was reacted in a 90 °C common H_3PO_4 bath for 8–10 min. Liberated CO_2 gas was collected and purified cryogenically. Sample gas and an in-house reference gas were analyzed four times each in the course of each measurement. The CM-2 Cararra Marble standard was measured seven times during each run of 53 samples to calibrate samples to the V-PDB standard, provide a measure of uncertainty, and monitor potential memory effect associated with the common acid bath system. Analytical uncertainties (1σ) for both $\delta^{13}C$ and δ^{18} O were < 0.1 ‰, and memory effect for $\delta^{13}C$ was consistently < 0.2 ‰.

3.2. $\delta^{13}C$ and δ^{18} O results

The carbon isotope curve for the Shaler Supergroup (Fig. 5) is a composite of 17 measured stratigraphic sections, correlated through field and map observations. The lower portion of the Wynniatt Formation is reproduced in two locations in the northeast domain (S1/S2 and S14/S6), and the tan carbonate member of the Kilian Formation is reproduced in both the northeast (S9) and southwest domains (05RAT53).

$\delta^{13}C$ of the upper Aok Formation sits between 2 and 3‰. The Boot Inlet Formation shows $\delta^{13}C$ oscillating between 3 and 6‰. The other carbonate formation of the Reynolds Point Group, the Jago Bay, was not sampled in this study. Samples from limestones in the uppermost Minto Inlet Formation have $\delta^{13}C$ clustered around −1 ‰. Above this there is a large stepwise jump to values over 4‰ in the lower Wynniatt Formation. The $\delta^{13}C$ of the Wynniatt fluctuates between 2 and 8‰ before taking a precipitous dive to −5 ‰ below a large diabase sill. Immediately above the sill, Wynnniatt $\delta^{13}C$ values return to a range between 6 and 8‰. The transition to the Kilian Formation initiates a gradual decline in $\delta^{13}C$ over several hundred meters, reaching a nadir of −4 ‰ in the tan carbonate member immediately underlying the first basalt flows of the Natkusiak Formation.

4. Discussion

4.1. Reliability of Neoproterozoic $\delta^{13}C$ measurements

The reproducibility of $\delta^{13}C$ signals in Neoproterozoic carbonates worldwide has demonstrated that $\delta^{13}C_{carb}$ is a generally robust geochemical proxy (e.g., Derry et al., 1992; Kaufman et al., 1991; Kaufman and Knoll, 1995). However, the fidelity of δ^{18} O values recorded in Neoproterozoic carbonates and their relationship to the δ^{18} O composition of the seawater in which they were precipitated is subject to much debate. Carbon in sedimentary carbonate rocks is buffered against significant isotopic exchange during rock–fluid interactions, but oxygen is not; the ratio of the amount of carbon

Table 1
Summary of $\delta^{13}C$ and δ^{18} O values measured in this study. "ls" = limestone and "dl" = dolomite.

Section number	Stratigraphic height (m)	$\delta^{13}C$ (‰, V-PDB)	$\delta^{18}O$ (‰, V-PDB)	Carbonate mineralogy	Formation
S1	8.2	4.71	−5.45	ls	Wynniatt
S1	8.7	4.69	−4.36	ls	Wynniatt
S1	9.2	4.44	−5.57	ls	Wynniatt
S1	10.2	3.89	−7.14	ls	Wynniatt
S1	10.7	4.48	−7.44	ls	Wynniatt
S1	11.7	5.20	−6.57	ls	Wynniatt
S1	12.9	5.06	−6.65	ls	Wynniatt
S1	13.4	4.69	−7.45	ls	Wynniatt
S1	13.8	5.34	−6.27	ls	Wynniatt
S1	14.5	5.77	−5.89	ls	Wynniatt
S1	15.6	4.53	−8.57	ls	Wynniatt
S1	16.6	4.89	−7.59	ls	Wynniatt
S1	17.6	5.29	−6.89	ls	Wynniatt
S1	18.2	4.09	−9.46	ls	Wynniatt
S1	18.9	4.22	−8.70	ls	Wynniatt
S1	19.9	4.63	−5.97	ls	Wynniatt
S1	20.3	4.11	−4.63	ls	Wynniatt
S1	20.8	3.72	−4.45	ls	Wynniatt
S1	21.9	3.43	−5.08	ls	Wynniatt
S1	22.5	3.77	−2.55	ls	Wynniatt
S1	23.3	3.36	−5.08	ls	Wynniatt
S1	23.9	2.06	−9.69	ls	Wynniatt
S1	24.3	3.45	−6.09	ls	Wynniatt
S1	25.5	2.35	−10.57	ls	Wynniatt
S1	25.6	2.39	−10.87	ls	Wynniatt
S1	27.2	3.34	−12.74	ls	Wynniatt
S1	28.2	1.40	−12.72	ls	Wynniatt
S1	32.3	2.27	−11.44	ls	Wynniatt
S1	32.9	3.33	−8.91	dl	Wynniatt
S1	33.7	3.90	−7.77	dl	Wynniatt
S1	34.5	3.17	−9.45	dl	Wynniatt
S1	35.5	3.88	−7.69	dl	Wynniatt
S1	36.2	3.93	−8.07	dl	Wynniatt
S1	36.7	4.08	−7.83	dl	Wynniatt
S1	37.2	3.80	−7.91	dl	Wynniatt
S1	37.7	3.81	−7.71	dl	Wynniatt
S1	38.2	4.45	−5.92	dl	Wynniatt
S1	38.7	3.60	−7.56	dl	Wynniatt
S1	39.2	3.64	−6.94	dl	Wynniatt
S1	39.7	3.69	−6.48	dl	Wynniatt
S1	40.2	3.48	−6.81	dl	Wynniatt
S1	40.7	3.18	−9.00	dl	Wynniatt
S1	41.7	3.83	−7.46	dl	Wynniatt
S1	42.2	3.40	−8.96	dl	Wynniatt
S1	43.3	3.22	−9.11	ls	Wynniatt
S1	44.1	2.49	−9.23	dl	Wynniatt
S1	61.3	4.05	−4.54	dl	Wynniatt
S1	62.1	4.24	−3.88	dl	Wynniatt
S1	62.6	4.19	−4.26	dl	Wynniatt
S1	63.6	4.09	−4.52	dl	Wynniatt
S1	64.3	2.58	−9.02	ls	Wynniatt
S1	64.9	4.02	−5.00	ls	Wynniatt
S2	1.5	4.31	−5.25	ls	Wynniatt
S2	2.4	4.61	−3.80	ls	Wynniatt
S2	3.0	4.64	−2.91	ls	Wynniatt
S2	4.0	4.93	−3.85	ls	Wynniatt
S2	4.5	4.74	−2.92	ls	Wynniatt
S2	5.1	4.99	−3.13	ls	Wynniatt
S2	5.6	4.32	−2.77	ls	Wynniatt
S2	6.3	4.33	−1.59	ls	Wynniatt
S2	6.8	4.56	−1.52	ls	Wynniatt
S2	7.2	4.26	−3.84	ls	Wynniatt
S2	8.5	4.08	−3.95	ls	Wynniatt
S2	10.1	6.24	−6.45	ls	Wynniatt
S2	10.5	6.56	−5.82	ls	Wynniatt
S2	11.0	5.41	−5.53	ls	Wynniatt
S2	11.5	5.84	−6.47	ls	Wynniatt
S2	12.0	6.69	−6.03	ls	Wynniatt
S2	12.8	6.42	−6.31	ls	Wynniatt
S2	13.4	6.53	−6.38	ls	Wynniatt
S2	14.1	6.38	−6.64	ls	Wynniatt
S2	15.6	6.53	−6.77	ls	Wynniatt
S2	16.6	6.50	−6.77	ls	Wynniatt

Table 1 (*Continued*)

Section number	Stratigraphic height (m)	$\delta^{13}C$ (‰, V-PDB)	$\delta^{18}O$ (‰, V-PDB)	Carbonate mineralogy	Formation
S2	17.1	6.09	−6.57	ls	Wynniatt
S2	17.6	6.27	−6.80	ls	Wynniatt
S2	18.0	6.98	−6.89	ls	Wynniatt
S2	18.5	6.74	−6.60	ls	Wynniatt
S2	18.9	7.35	−5.25	ls	Wynniatt
S2	20.1	7.04	−5.30	ls	Wynniatt
S2	20.7	7.46	−5.28	ls	Wynniatt
S2	21.2	7.78	−5.12	ls	Wynniatt
S2	21.8	7.58	−5.08	ls	Wynniatt
S2	22.4	7.71	−5.70	ls	Wynniatt
S2	23.1	7.60	−5.60	ls	Wynniatt
S2	23.7	7.41	−5.29	ls	Wynniatt
S2	24.8	7.37	−5.27	ls	Wynniatt
S2	25.3	7.75	−5.49	ls	Wynniatt
S2	25.8	7.69	−5.20	ls	Wynniatt
S2	26.8	7.57	−5.35	ls	Wynniatt
S2	27.6	6.55	−6.38	ls	Wynniatt
S2	28.1	7.69	−5.59	ls	Wynniatt
S2	28.7	7.05	−7.09	ls	Wynniatt
S2	29.3	8.18	−5.83	ls	Wynniatt
S2	30.0	8.12	−6.01	ls	Wynniatt
S2	30.5	8.18	−5.76	ls	Wynniatt
S2	31.0	7.90	−6.11	ls	Wynniatt
S2	31.5	7.16	−6.46	ls	Wynniatt
S2	33.6	6.85	−6.18	ls	Wynniatt
S2	36.3	6.30	−6.27	ls	Wynniatt
S2	36.9	6.25	−6.23	ls	Wynniatt
S2	37.6	6.28	−6.37	ls	Wynniatt
S2	38.5	6.29	−6.51	ls	Wynniatt
S2	39.3	6.98	−6.68	ls	Wynniatt
S2	50.7	6.44	−6.46	ls	Wynniatt
S2	51.8	5.56	−6.74	ls	Wynniatt
S2	51.9	5.84	−7.41	ls	Wynniatt
S2	52.6	5.73	−6.96	ls	Wynniatt
S2	53.2	5.67	−7.20	ls	Wynniatt
S2	53.7	5.76	−7.00	ls	Wynniatt
S2	55.0	4.75	−7.65	ls	Wynniatt
S2	55.6	4.75	−7.43	ls	Wynniatt
S2	56.2	4.58	−7.60	ls	Wynniatt
S2	57.0	4.75	−7.59	ls	Wynniatt
S2	57.9	5.06	−7.58	ls	Wynniatt
S2	58.5	5.04	−7.52	ls	Wynniatt
S2	59.3	4.95	−7.95	ls	Wynniatt
S2	59.4	5.78	−7.12	ls	Wynniatt
S2	59.8	5.40	−7.22	ls	Wynniatt
S2	60.7	5.61	−7.15	ls	Wynniatt
S2	61.3	5.38	−7.16	ls	Wynniatt
S2	62.7	5.38	−7.33	ls	Wynniatt
S2	63.4	5.49	−6.87	ls	Wynniatt
S2	64.1	5.50	−7.14	ls	Wynniatt
S2	64.8	5.86	−6.39	ls	Wynniatt
S2	65.4	4.61	−7.62	ls	Wynniatt
S2	66.0	4.39	−8.37	ls	Wynniatt
S2	66.5	4.27	−9.51	ls	Wynniatt
S2	67.6	4.12	−9.10	ls	Wynniatt
S2	68.8	4.30	−8.70	ls	Wynniatt
S2	70.0	4.64	−9.28	ls	Wynniatt
S2	70.9	4.71	−9.49	ls	Wynniatt
S2	71.7	4.57	−9.48	ls	Wynniatt
S2	72.8	4.50	−9.39	ls	Wynniatt
S2	73.5	4.41	−9.28	ls	Wynniatt
S2	74.9	5.12	−8.21	ls	Wynniatt
S2	75.6	5.01	−8.17	ls	Wynniatt
S2	76.2	4.85	−8.21	ls	Wynniatt
S2	77.7	4.46	−7.87	ls	Wynniatt
S2	78.6	4.38	−8.13	ls	Wynniatt
S2	79.4	4.53	−8.27	ls	Wynniatt
S2	80.2	3.68	−9.21	ls	Wynniatt
S2	81.5	2.88	−9.21	ls	Wynniatt
S2	82.1	3.55	−9.17	ls	Wynniatt
S2	83.1	4.89	−8.00	ls	Wynniatt
S2	84.4	1.35	−11.48	ls	Wynniatt
S2	85.3	1.07	−11.31	ls	Wynniatt
S2	86.3	1.66	−10.05	ls	Wynniatt
S2	87.8	4.84	−8.99	ls	Wynniatt

Table 1 (*Continued*)

Section number	Stratigraphic height (m)	$\delta^{13}C$ (‰, V-PDB)	$\delta^{18}O$ (‰, V-PDB)	Carbonate mineralogy	Formation
S2	89.0	4.50	−9.03	ls	Wynniatt
S2	90.0	3.97	−9.00	ls	Wynniatt
S2	90.9	4.42	−8.70	ls	Wynniatt
S2	91.0	5.92	−8.22	ls	Wynniatt
S2	92.0	4.72	−10.03	ls	Wynniatt
S2	93.5	3.20	−11.07	ls	Wynniatt
S2	94.7	6.20	−8.54	ls	Wynniatt
S2	96.0	4.16	−9.71	ls	Wynniatt
S2	98.0	4.86	−9.26	ls	Wynniatt
S2	101.0	4.07	−8.42	ls	Wynniatt
S2	102.0	3.83	−6.71	ls	Wynniatt
S2	103.5	4.95	−5.26	ls	Wynniatt
S2	105.0	2.38	−9.47	ls	Wynniatt
S2	106.5	1.49	−11.80	ls	Wynniatt
S2	108.5	−4.15	−10.16	ls	Wynniatt
S2	110.3	−5.17	−10.61	ls	Wynniatt
S2	111.8	−0.65	−11.09	ls	Wynniatt
S2	114.5	−4.99	−10.28	ls	Wynniatt
S4	0.3	5.16	−5.53	dl	Wynniatt
S4	0.9	5.11	−5.69	dl	Wynniatt
S4	1.1	4.34	−6.61	dl	Wynniatt
S4	1.8	4.42	−5.91	dl	Wynniatt
S4	2.3	4.32	−5.85	dl	Wynniatt
S4	3.0	4.43	−6.01	dl	Wynniatt
S4	3.4	4.45	−5.32	dl	Wynniatt
S4	3.7	4.45	−5.86	dl	Wynniatt
S4	4.4	4.53	−6.19	dl	Wynniatt
S4	4.9	4.28	−6.53	dl	Wynniatt
S4	5.2	4.14	−6.32	dl	Wynniatt
S4	5.5	4.33	−5.69	dl	Wynniatt
S6	0.5	3.94	−4.64	ls	Wynniatt
S6	1.0	5.24	−7.83	ls	Wynniatt
S6	1.2	5.18	−7.82	ls	Wynniatt
S6	1.8	5.19	−8.49	ls	Wynniatt
S6	2.3	4.98	−8.31	ls	Wynniatt
S6	2.7	5.22	−8.31	ls	Wynniatt
S6	3.1	4.82	−8.25	ls	Wynniatt
S6	3.6	4.99	−8.12	ls	Wynniatt
S6	3.9	4.96	−7.89	ls	Wynniatt
S6	4.3	5.05	−8.06	ls	Wynniatt
S6	4.8	5.16	−7.45	ls	Wynniatt
S6	5.2	5.02	−7.19	ls	Wynniatt
S6	5.6	5.10	−7.11	ls	Wynniatt
S6	6.3	5.42	−7.30	ls	Wynniatt
S6	6.8	5.39	−7.39	ls	Wynniatt
S6	7.3	5.11	−7.10	ls	Wynniatt
S6	7.8	5.09	−7.07	ls	Wynniatt
S6	8.3	5.08	−7.11	ls	Wynniatt
S6	8.7	5.31	−6.95	ls	Wynniatt
S6	9.1	5.21	−6.90	ls	Wynniatt
S6	9.4	5.29	−6.70	ls	Wynniatt
S6	9.9	5.48	−6.69	ls	Wynniatt
S6	10.5	5.29	−6.55	ls	Wynniatt
S6	10.9	5.29	−6.75	ls	Wynniatt
S6	11.3	5.28	−6.62	ls	Wynniatt
S6	11.6	5.37	−6.72	ls	Wynniatt
S6	11.8	5.01	−6.37	ls	Wynniatt
S6	12.1	5.43	−6.68	ls	Wynniatt
S6	12.8	5.59	−6.40	ls	Wynniatt
S6	13.4	5.40	−6.68	ls	Wynniatt
S6	13.8	5.44	−6.69	ls	Wynniatt
S6	14.2	5.50	−6.69	ls	Wynniatt
S6	14.7	5.26	−6.78	ls	Wynniatt
S6	15.0	5.19	−6.70	ls	Wynniatt
S6	15.3	5.05	−7.17	dl	Wynniatt
S6	15.8	5.69	−7.18	ls	Wynniatt
S6	16.2	5.65	−6.60	ls	Wynniatt
S6	16.7	5.93	−6.32	ls	Wynniatt
S6	17.2	6.15	−6.73	ls	Wynniatt
S6	17.7	6.77	−6.47	ls	Wynniatt
S6	18.2	7.11	−6.15	ls	Wynniatt
S6	18.7	7.01	−6.07	ls	Wynniatt
S6	19.2	6.91	−6.53	ls	Wynniatt
S6	19.6	6.40	−6.50	ls	Wynniatt

Table 1 (*Continued*)

Section number	Stratigraphic height (m)	$\delta^{13}C$ (‰, V-PDB)	$\delta^{18}O$ (‰, V-PDB)	Carbonate mineralogy	Formation
S6	20.2	6.60	−6.53	ls	Wynniatt
S6	20.7	7.15	−6.34	ls	Wynniatt
S6	21.3	6.69	−6.75	ls	Wynniatt
S6	21.9	7.07	−6.45	ls	Wynniatt
S6	22.3	6.66	−6.63	ls	Wynniatt
S6	22.8	6.73	−6.54	ls	Wynniatt
S6	23.4	6.56	−6.77	ls	Wynniatt
S6	23.9	6.55	−7.52	ls	Wynniatt
S6	24.3	6.91	−6.72	ls	Wynniatt
S6	24.8	6.25	−6.60	ls	Wynniatt
S6	25.1	6.15	−6.78	dl	Wynniatt
S6	25.7	6.43	−7.00	ls	Wynniatt
S6	26.1	6.19	−6.56	ls	Wynniatt
S6	26.5	6.28	−6.93	ls	Wynniatt
S6	27.0	5.95	−7.75	ls	Wynniatt
S6	27.5	6.10	−7.73	ls	Wynniatt
S6	28.0	5.77	−7.63	ls	Wynniatt
S6	28.2	5.79	−7.53	ls	Wynniatt
S6	29.2	5.71	−6.54	ls	Wynniatt
S7	0.2	6.13	−5.86	ls	Wynniatt
S7	0.8	6.24	−5.19	ls	Wynniatt
S7	1.2	6.05	−5.19	ls	Wynniatt
S7	1.6	6.28	−5.67	ls	Wynniatt
S7	2.1	6.31	−5.76	ls	Wynniatt
S7	2.6	5.83	−6.11	ls	Wynniatt
S7	3.2	5.77	−5.96	ls	Wynniatt
S7	3.8	5.35	−6.21	ls	Wynniatt
S7	4.3	6.02	−6.69	ls	Wynniatt
S7	4.9	6.24	−6.49	ls	Wynniatt
S7	5.3	5.86	−6.31	ls	Wynniatt
S7	5.9	5.70	−7.60	ls	Wynniatt
S7	6.5	5.73	−7.76	ls	Wynniatt
S7	6.9	6.35	−6.32	ls	Wynniatt
S7	7.5	5.69	−7.49	ls	Wynniatt
S7	8.0	6.64	−5.69	ls	Wynniatt
S7	8.6	5.90	−6.37	ls	Wynniatt
S7	9.2	5.52	−7.72	ls	Wynniatt
S7	10.0	5.53	−6.27	ls	Wynniatt
S7	10.5	6.37	−5.80	ls	Wynniatt
S7	10.9	5.30	−7.91	ls	Wynniatt
S7	11.5	6.26	−6.46	ls	Wynniatt
S7	12.0	5.79	−7.24	ls	Wynniatt
S7	12.6	5.56	−7.26	ls	Wynniatt
S7	13.2	6.30	−5.64	ls	Wynniatt
S7	13.6	6.12	−5.80	ls	Wynniatt
S7	15.1	6.45	−5.15	ls	Wynniatt
S7	15.7	6.24	−6.28	ls	Wynniatt
S7	16.2	6.29	−6.16	ls	Wynniatt
S7	16.6	5.79	−6.42	ls	Wynniatt
S7	17.2	6.37	−5.57	ls	Wynniatt
S7	17.5	6.22	−5.00	ls	Wynniatt
S7	17.9	6.19	−4.87	ls	Wynniatt
S7	18.5	6.11	−4.70	ls	Wynniatt
S7	19.0	6.03	−5.19	ls	Wynniatt
S7	19.4	5.97	−5.02	ls	Wynniatt
S7	19.7	5.94	−5.06	ls	Wynniatt
S9	0.1	1.65	−9.19	ls	Kilian
S9	1.3	1.87	−10.12	ls	Kilian
S9	4.3	0.89	−10.42	ls	Kilian
S9	5.0	0.72	−10.31	ls	Kilian
S9	32.3	−0.41	−3.64	dl	Kilian
S9	33.3	0.42	−4.71	dl	Kilian
S9	35.5	0.74	−3.65	dl	Kilian
S9	35.9	0.76	−4.03	dl	Kilian
S9	36.4	1.06	−4.13	dl	Kilian
S9	38.7	0.55	−4.35	dl	Kilian
S9	50.3	1.96	−4.41	dl	Kilian
S9	50.8	1.37	−2.96	dl	Kilian
S9	52.2	−0.38	−2.95	dl	Kilian
S9	52.7	0.82	−3.75	dl	Kilian
S9	54.6	1.14	−4.28	dl	Kilian
S9	59.6	−1.99	−4.03	dl	Kilian
S9	66.4	−0.35	−3.19	dl	Kilian
S9	68.2	−1.69	−3.70	dl	Kilian

Table 1 (*Continued*)

Section number	Stratigraphic height (m)	$\delta^{13}C$ (‰, V-PDB)	$\delta^{18}O$ (‰, V-PDB)	Carbonate mineralogy	Formation
S9	73.2	−0.23	−3.52	dl	Kilian
S9	89.0	−2.50	−9.36	ls	Kilian
S9	89.5	−2.32	−11.57	ls	Kilian
S9	89.8	−3.51	−8.93	ls	Kilian
S9	90.3	−3.72	−9.96	ls	Kilian
S9	91.7	−4.06	−9.30	ls	Kilian
S9	92.2	−3.92	−9.39	ls	Kilian
S10	1.6	6.51	−5.75	ls	Wynniatt
S10	2.3	6.04	−5.78	ls	Wynniatt
S10	3.0	6.32	−5.67	ls	Wynniatt
S10	3.6	6.30	−5.95	ls	Wynniatt
S10	4.2	6.16	−5.79	ls	Wynniatt
S10	4.8	6.10	−5.91	ls	Wynniatt
S10	5.3	5.86	−6.37	ls	Wynniatt
S10	5.8	6.20	−6.20	ls	Wynniatt
S10	6.4	6.11	−6.04	ls	Wynniatt
S10	7.0	6.56	−5.97	ls	Wynniatt
S10	9.2	6.18	−5.74	ls	Wynniatt
S10	9.8	6.29	−6.18	ls	Wynniatt
S10	10.4	6.55	−6.07	ls	Wynniatt
S10	10.9	7.04	−5.99	ls	Wynniatt
S10	12.1	7.15	−5.70	ls	Wynniatt
S11	0.2	6.03	−7.44	ls	Wynniatt
S11	0.7	6.28	−7.38	ls	Wynniatt
S11	1.3	6.77	−7.09	ls	Wynniatt
S11	2.0	7.30	−7.04	ls	Wynniatt
S11	3.0	7.18	−7.11	ls	Wynniatt
S11	3.7	7.49	−6.90	ls	Wynniatt
S11	4.7	7.77	−6.69	ls	Wynniatt
S11	5.3	7.96	−6.42	ls	Wynniatt
S11	5.8	7.28	−6.50	ls	Wynniatt
S11	6.6	7.71	−6.64	ls	Wynniatt
S11	7.1	7.55	−6.59	ls	Wynniatt
S11	7.7	7.31	−6.52	ls	Wynniatt
S11	8.2	7.60	−6.54	ls	Wynniatt
S11	8.6	7.44	−6.48	ls	Wynniatt
S14	6.0	1.95	−9.53	ls	Wynniatt
S14	6.8	2.53	−9.51	ls	Wynniatt
S14	7.4	2.75	−9.30	ls	Wynniatt
S14	8.2	3.17	−9.06	ls	Wynniatt
S14	8.9	3.04	−7.70	ls	Wynniatt
S14	11.7	4.76	−4.54	dl	Wynniatt
S14	12.6	4.43	−5.32	dl	Wynniatt
S14	13.4	4.02	−5.32	ls	Wynniatt
S14	14.1	4.12	−3.76	dl	Wynniatt
S14	16.4	6.46	−6.40	ls	Wynniatt
S14	17.1	6.34	−6.40	ls	Wynniatt
S14	17.7	6.10	−6.54	ls	Wynniatt
S14	18.4	6.56	−6.26	ls	Wynniatt
S14	19.1	6.76	−6.28	ls	Wynniatt
S14	20.0	6.50	−6.66	ls	Wynniatt
S14	20.8	6.44	−6.51	ls	Wynniatt
S14	21.6	6.48	−6.45	ls	Wynniatt
S14	22.2	6.37	−7.14	ls	Wynniatt
S14	23.1	6.14	−5.73	ls	Wynniatt
S14	23.9	7.01	−5.76	ls	Wynniatt
S14	24.7	5.35	−5.74	ls	Wynniatt
S14	25.5	6.68	−5.86	ls	Wynniatt
S14	26.4	7.31	−5.64	ls	Wynniatt
S14	27.2	7.42	−6.55	ls	Wynniatt
S14	27.9	7.32	−6.04	ls	Wynniatt
S14	28.7	7.22	−6.22	ls	Wynniatt
S14	29.4	7.31	−6.14	ls	Wynniatt
S14	30.2	7.26	−5.84	ls	Wynniatt
S14	31.0	7.56	−5.91	ls	Wynniatt
S14	31.8	7.63	−6.28	ls	Wynniatt
S14	32.6	7.84	−6.44	ls	Wynniatt
S14	33.4	7.91	−6.10	ls	Wynniatt
S14	34.2	7.08	−6.91	ls	Wynniatt
S14	35.1	6.82	−6.53	ls	Wynniatt
S14	35.8	6.82	−6.34	ls	Wynniatt
S14	36.5	6.86	−5.99	ls	Wynniatt
S14	37.2	6.86	−6.00	ls	Wynniatt

Table 1 (*Continued*)

Section number	Stratigraphic height (m)	$\delta^{13}C$ (‰, V-PDB)	$\delta^{18}O$ (‰, V-PDB)	Carbonate mineralogy	Formation
S14	37.9	6.20	−6.30	ls	Wynniatt
S14	38.7	6.07	−6.31	ls	Wynniatt
S14	39.4	6.84	−6.12	ls	Wynniatt
S14	40.2	6.17	−6.05	ls	Wynniatt
S14	40.9	5.99	−6.06	ls	Wynniatt
S14	41.5	6.67	−6.45	ls	Wynniatt
S14	42.2	6.81	−5.49	ls	Wynniatt
S14	42.9	6.13	−5.47	ls	Wynniatt
S14	43.6	5.93	−5.71	ls	Wynniatt
S14	44.3	5.97	−5.72	ls	Wynniatt
S14	45.0	6.78	−6.30	ls	Wynniatt
S14	45.7	6.34	−6.38	ls	Wynniatt
S14	46.6	5.57	−6.77	ls	Wynniatt
S14	47.4	5.95	−7.20	ls	Wynniatt
S14	48.1	5.39	−7.20	ls	Wynniatt
S14	48.8	4.76	−7.15	ls	Wynniatt
S14	49.4	4.86	−8.05	ls	Wynniatt
S14	50.1	5.08	−7.80	ls	Wynniatt
S14	50.8	5.13	−7.78	ls	Wynniatt
S14	51.5	5.25	−7.79	ls	Wynniatt
S14	52.2	5.35	−7.45	ls	Wynniatt
S14	52.9	5.47	−7.26	ls	Wynniatt
S14	53.5	5.13	−7.26	ls	Wynniatt
S14	54.3	5.51	−7.31	ls	Wynniatt
S14	55.0	5.40	−7.34	ls	Wynniatt
S14	55.7	5.67	−7.23	ls	Wynniatt
S14	55.7	5.60	−7.27	ls	Wynniatt
S14	56.4	5.53	−7.14	ls	Wynniatt
S14	57.2	5.53	−7.18	ls	Wynniatt
S14	57.9	5.35	−7.47	ls	Wynniatt
S14	58.6	5.40	−7.29	ls	Wynniatt
S14	59.0	5.85	−6.14	dl	Wynniatt
S14	59.7	4.94	−7.46	ls	Wynniatt
S14	60.3	4.67	−7.85	ls	Wynniatt
S14	60.5	4.80	−7.85	ls	Wynniatt
S14	61.3	4.51	−7.94	ls	Wynniatt
S14	62.0	4.30	−8.32	ls	Wynniatt
S14	63.4	4.23	−8.67	ls	Wynniatt
S14	64.1	4.32	−8.47	ls	Wynniatt
S14	64.8	4.39	−8.51	ls	Wynniatt
S14	65.6	4.47	−8.83	ls	Wynniatt
S14	66.3	4.75	−8.87	ls	Wynniatt
S14	67.1	4.89	−8.05	ls	Wynniatt
S14	67.8	5.26	−7.69	ls	Wynniatt
S14	68.5	5.30	−7.78	ls	Wynniatt
S14	68.5	5.27	−7.80	ls	Wynniatt
S14	69.2	4.75	−9.38	ls	Wynniatt
S14	69.2	4.73	−9.39	ls	Wynniatt
S14	69.8	4.98	−8.16	ls	Wynniatt
S14	69.8	4.96	−8.16	ls	Wynniatt
S15	0.8	2.24	−8.07	ls	Aok
S15	1.2	2.19	−8.86	ls	Aok
S15	2.1	2.48	−8.18	ls	Aok
S15	4.1	2.04	−9.36	ls	Aok
S15	4.1	2.01	−9.38	ls	Aok
S15	5.3	2.28	−7.69	ls	Aok
S15	6.1	2.38	−8.63	ls	Aok
S15	7.3	2.40	−9.20	ls	Aok
S15	8.8	2.10	−8.81	ls	Aok
S15	9.5	2.30	−9.21	ls	Aok
S15	10.3	2.15	−9.51	ls	Aok
S15	11.6	2.30	−9.10	ls	Aok
S15	12.4	2.36	−9.18	ls	Aok
S15	13.3	2.94	−8.37	ls	Aok
S15	14.0	2.67	−8.02	ls	Aok
S15	15.8	1.96	−7.29	ls	Aok
S15	16.6	2.01	−7.24	ls	Aok
S15	17.2	2.14	−7.08	ls	Aok
S15	18.3	1.99	−7.41	ls	Aok
S15	19.1	2.12	−7.51	ls	Aok
S15	20.4	2.52	−7.19	ls	Aok
S15	21.5	2.70	−8.14	ls	Aok
S15	22.1	2.61	−7.34	ls	Aok
S15	23.4	2.79	−7.87	ls	Aok
S15	24.8	3.15	−7.14	ls	Aok
S15	25.4	3.10	−7.78	ls	Aok

Table 1 (*Continued*)

Section number	Stratigraphic height (m)	$\delta^{13}C$ (‰, V-PDB)	$\delta^{18}O$ (‰, V-PDB)	Carbonate mineralogy	Formation
S15	26.5	3.12	−7.94	Is	Aok
S16	0.9	4.16	−8.15	Is	Boot Inlet
S16	1.6	4.19	−8.28	Is	Boot Inlet
S16	2.6	4.34	−7.96	Is	Boot Inlet
S16	3.3	4.30	−7.94	Is	Boot Inlet
S16	4.1	4.20	−7.99	Is	Boot Inlet
S16	5.3	4.16	−7.98	Is	Boot Inlet
S16	6.5	4.18	−7.75	Is	Boot Inlet
S16	7.4	4.22	−7.82	Is	Boot Inlet
S16	8.1	3.80	−7.89	Is	Boot Inlet
S16	17.2	4.23	−7.20	Is	Boot Inlet
S16	19.2	4.61	−7.43	Is	Boot Inlet
S16	20.1	4.75	−8.19	Is	Boot Inlet
S16	22.3	4.57	−8.57	Is	Boot Inlet
S16	29.5	0.94	−9.05	Is	Boot Inlet
S16	31.0	0.63	−9.24	Is	Boot Inlet
S16	32.3	3.63	−8.23	Is	Boot Inlet
S16	33.6	4.73	−8.42	Is	Boot Inlet
S16	34.4	4.77	−7.92	Is	Boot Inlet
S16	40.8	5.02	−6.14	Is	Boot Inlet
S16	41.7	5.09	−6.09	Is	Boot Inlet
S16	42.5	5.06	−6.96	Is	Boot Inlet
S16	43.2	5.01	−7.17	Is	Boot Inlet
S16	44.9	4.87	−6.39	Is	Boot Inlet
S16	45.6	4.43	−6.57	Is	Boot Inlet
S16	46.5	4.56	−5.85	Is	Boot Inlet
S16	48.6	4.73	−7.71	Is	Boot Inlet
S16	49.9	4.62	−7.55	Is	Boot Inlet
S16	50.8	4.56	−7.11	Is	Boot Inlet
S16	51.7	4.64	−6.97	Is	Boot Inlet
S16	52.8	4.21	−7.47	Is	Boot Inlet
S16	54.9	4.43	−7.18	Is	Boot Inlet
S16	55.3	4.46	−7.36	Is	Boot Inlet
S16	56.5	4.07	−8.13	Is	Boot Inlet
S16	58.9	4.40	−7.14	Is	Boot Inlet
S16	59.7	4.18	−6.74	Is	Boot Inlet
S16	60.8	4.08	−7.33	Is	Boot Inlet
S16	61.4	3.25	−6.77	Is	Boot Inlet
S16	62.4	3.40	−7.38	Is	Boot Inlet
S16	63.2	3.71	−6.48	Is	Boot Inlet
S16	64.3	3.48	−6.65	Is	Boot Inlet
S16	65.1	3.77	−6.55	Is	Boot Inlet
S16	66.0	3.97	−7.44	Is	Boot Inlet
S16	67.1	4.26	−6.79	Is	Boot Inlet
S16	68.0	4.20	−6.32	Is	Boot Inlet
S16	69.0	4.25	−6.89	Is	Boot Inlet
S16	79.7	4.25	−5.95	Is	Boot Inlet
S16	81.7	4.87	−5.82	Is	Boot Inlet
S16	83.0	4.78	−6.42	Is	Boot Inlet
S16	85.8	4.33	−6.46	Is	Boot Inlet
S16	89.0	4.08	−5.85	Is	Boot Inlet
S16	91.5	3.97	−6.98	Is	Boot Inlet
S16	92.9	3.83	−6.66	Is	Boot Inlet
S16	95.9	3.93	−6.27	Is	Boot Inlet
S16	97.7	3.50	−6.42	Is	Boot Inlet
S16	100.0	3.85	−5.47	Is	Boot Inlet
S16	104.0	3.80	−5.60	Is	Boot Inlet
S16	110.0	4.57	−6.33	Is	Boot Inlet
S16	114.3	4.59	−6.94	Is	Boot Inlet
S16	116.1	4.69	−5.29	Is	Boot Inlet
S16	119.4	4.90	−6.75	Is	Boot Inlet
S16	122.9	5.38	−6.45	Is	Boot Inlet
S16	124.0	4.98	−6.54	Is	Boot Inlet
S16	129.3	4.38	−7.69	Is	Boot Inlet
S16	131.0	4.66	−7.37	Is	Boot Inlet
S16	132.4	4.42	−7.15	Is	Boot Inlet
S16	133.5	4.39	−6.83	Is	Boot Inlet
05RAT53	0	−2.83	−11.58		Kilian
05RAT53	3	−2.97	−9.50		Kilian
05RAT53	6	−3.17	−8.56		Kilian
05RAT53	9	−4.20	−8.13		Kilian
05RAT53	12	−4.14	−8.15		Kilian
05RAT53	27	−3.55	−7.46		Kilian
05RAT53	29	−3.53	−7.65		Kilian
05RAT53	35	−2.71	−7.61		Kilian

Table 1 (*Continued*)

Section number	Stratigraphic height (m)	$\delta^{13}C$ (‰, V-PDB)	$\delta^{18}O$ (‰, V-PDB)	Carbonate mineralogy	Formation
05RAT53	38	−2.47	−7.67		Kilian
05RAT53	41	−1.21	−7.55		Kilian
05RAT53	44	−2.05	−7.53		Kilian
05RAT53	51	−2.13	−5.98		Kilian
05RAT53	60	−3.67	−4.89		Kilian
05RAT53	64	−2.96	−5.05		Kilian
05RAT53	67	−2.68	−4.87		Kilian
05RAT53	69	−2.91	−4.98		Kilian
05RAT53	90	−1.07	−4.36		Kilian
05RAT53	93	−0.84	−4.78		Kilian
05RAT53	96	−1.37	−4.25		Kilian

Table 2
GPS coordinates of measured sections.

Section number	Latitude	Longitude
S1	N 72°13.261′	W111°41.146′
S2	N 72°13.065′	W111°41.730′
S4	N 72°07.219′	W111°38.583′
S6	N 72°11.718′	W111°43.560′
S7	N 72°10.836′	W111°40.872′
S8	N 72°11.275′	W111°45.549′
S9	N 72°03.669′	W111°49.442′
S10	N 72°09.315′	W111°38.689′
S11	N 72°09.765′	W111°38.968′
S12	N 72°12.315′	W111°47.210′
S13	N 72°11.993′	W111°48.857′
S14	N 72°11.876′	W111°43.765′
S15	N 72°15.945′	W109°59.367′
S16	N 72°17.080′	W109°58.488′

in the rocks to the amount of carbon dissolved in fluids is orders of magnitude higher than the ratio for oxygen. Therefore, the oxygen isotopic composition of carbonate rocks is subject to resetting through a host of post-depositional processes including meteoric diagenesis.

Like most Neoproterozoic carbonates worldwide, the samples from the Shaler Supergroup are highly depleted in δ^{18} O (mean value of -7.0 ± 1.6 ‰), raising the issue of whether the $\delta^{13}C$ and δ^{18} O of the samples reflect a primary signal, or whether the original $\delta^{13}C$ and δ^{18} O values have been significantly altered by diagenesis. Analysis of covariation of $\delta^{13}C$–δ^{18} O in the measured sections shows that there is usually some degree of positive correlation (Table 3). Such isotopic covariation has been argued to represent diagenetic overprinting. However, diagenetic overprinting is not the only mechanism that produces $\delta^{13}C$–δ^{18} O covariation, and occurrence of such correlation does not require diagenetic overprinting of the $\delta^{13}C$ signal.

A possible rationale for questioning the validity of the upper portion of section S2 is that it is capped by a ~50 m thick diabase sill, which could have introduced hydrothermal fluid to some portion of the upper part of S2; limestones in the 5 m immediately below the sill have been strongly metasomatized, and it is noted that the $\delta^{13}C$ dives to depleted values in the 10 m below the sill. However, isotopic covariation is not observed beneath any of the other sills that intrude the Shaler Supergroup in this study, and the other sections that do demonstrate covariation are not close to any sills. Moreover, the isotopic depletion is one-sided (observed immediately beneath sills but not above); any metasomatic isotopic alteration should be two-sided unless the sill acts as a cap and sets up a closed convection system below. At section S16, a 6-m thick diabase sill intrudes the Boot Inlet Formation, yet limestones in contact with it immediately above and immediately below demonstrate no enrichment or depletion in $\delta^{13}C$ (see section S16 in Fig. 5, above meter level 200). Therefore, it is unlikely that hydrothermal fluids accompanying intrusion of the sills are related to the isotopic covariations or $\delta^{13}C$ depletions.

Table 3
Summary of δ^{18} O vs. $\delta^{13}C$ covariation parameters for measured sections.

Section	Slope (d18O/d13C)	r^2	n
S1	1.49	0.35	52
S2	0.5	0.31	114
S4	0.64	0.26	12
S6	0.27	0.09	63
S7	1.69	0.38	37
S9	0.63	0.16	25
S10	0.18	0.1	16
S11	0.53	0.72	14
S12	0.64	0.66	5
S14	0.61	0.4	87
S15	0.52	0.05	27
S16	0.42	0.14	66

Contact metamorphism and subsequent decarbonation can lead to depletion in $\delta^{13}C$, necessitating an examination of the negative $\delta^{13}C$ anomalies in S2 and S9 for geochemical evidence of decarbonation. Although they are not well constrained due to weak correlation between $\delta^{13}C$ and $\delta^{18}O$, the $\delta^{18}O/\delta^{13}C$ slope in the upper portion of S2 and S9 are 0.55 and 0.63, which do not match slopes of 2 found in theoretical and empirical studies of decarbonated rocks (Shieh and Taylor, 1969; Boulvais et al., 1998). The magnitude of $\delta^{13}C$ depletion in both sections is ~10 ‰. Such intense depletion can occur in carbon-limited systems with near complete decarbonation. However, the Shaler samples have a low detrital silica content, and thus the depletion of $\delta^{13}C$ due to decarbonation reactions is probably no greater than 1‰. Therefore, the negative anomalies cannot be explained by contact metamorphism from basalt flows (S9) or diabase sills (S2), and the $\delta^{13}C$ anomalies are parsimoniously interpreted as primary ocean signals.

A comparison of the isotopic measurements from the tan carbonate member in the northeast (section S9) and the southwest (section 05RAT53) domains provides a further test of the reliability of the $\delta^{13}C$ signal. Although they are separated by 200 km (present coordinates), both sections record a negative isotope anomaly within the tan carbonate member, with values measured between −2 and −4 ‰ (Fig. 5). This is a strong positive result on a test of $\delta^{13}C$ coherence across the Amundsen Basin, especially in light of the fact that the samples from the southwest domain are more than 100 m below the nearest basalt flow whereas the northeast samples are immediately below a basalt flow.

In addition, a previous study of the geochemistry of Shaler Supergroup carbonates demonstrated that $\delta^{13}C$ was not correlated to variations in Mn/Sr (Asmerom et al., 1991). This is an indication that meteoric diagenesis, which tends to increase Mn/Sr, did not alter $\delta^{13}C$. Because the samples studied by Asmerom et al. (1991) were taken from the same locations as the samples in the present contribution, they provide additional confidence that the $\delta^{13}C$ data reported here are primary.

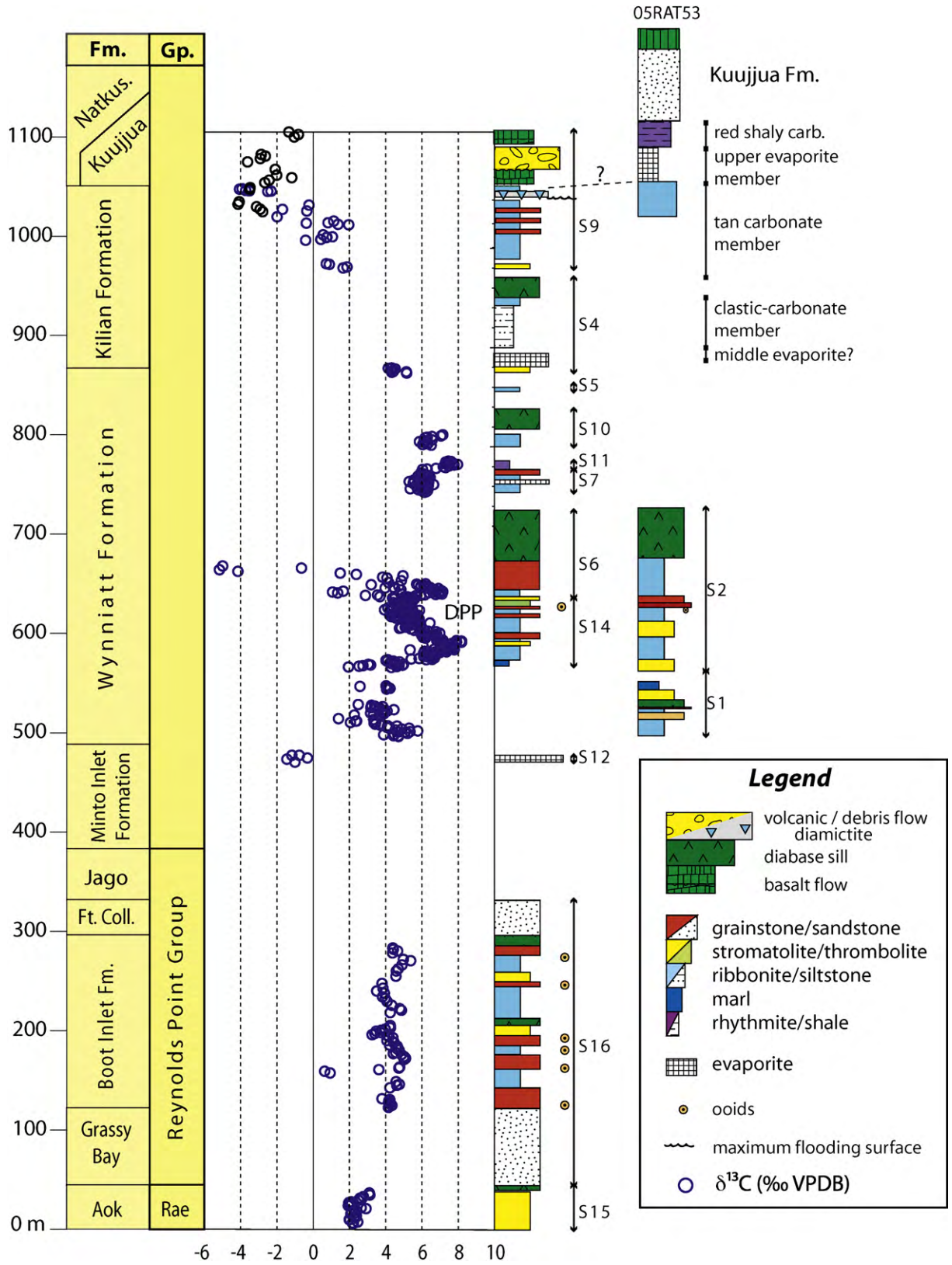

Fig. 5. Composite carbon isotope curve for the Shaler Supergroup plotted alongside simplified lithostratigraphy of measured sections (see Fig. 1 for locations). Sections numbered S*n* are in the northeastern Minto Inlier, where the Kuujjua Formation is absent. Section 05RAT53 is in the southwest domain (see Fig. 1 for location). DPP = "double positive peaks" referenced in text.

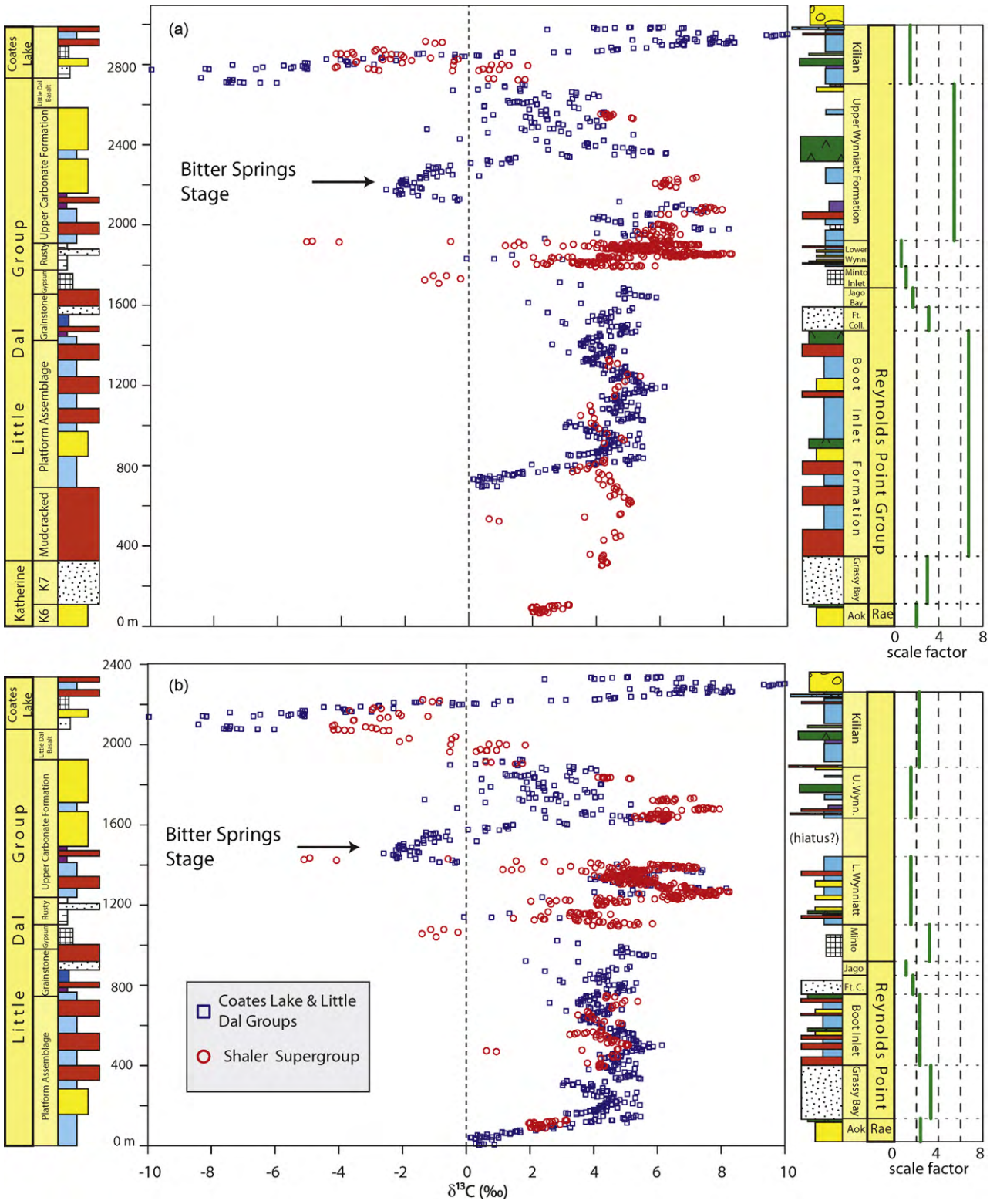

Fig. 6. (a) Formation-by-formation lithostratigraphic correlation of Shaler Supergroup with Mackenzie Mountains, after Rainbird et al. (1996), (b) Chemostratigraphic correlation based on $\delta^{13}C$. Stratigraphic height scaled to the thicker sections in the Mackenzie Mountains. The factor by which each formation of the Shaler Supergroup was scaled in order to match the thickness of the correlative unit is indicated to the right of each figure and labeled "scaling factor." In (a) the scaling factor varies between units by as much as a factor of 10, with some units requiring expansion and others compression. In (b) the scaling factors are much more consistent, and each is an expansion. The "Bitter Springs Stage" refers to the anomalously low set of $\delta^{13}C$ values in the Mackenzie Mountains Supergroup. See Fig. 5 for legend. Mackenzie Mountains Supergroup data, including location of BSS, from Halverson (2006) and Halverson et al. (2007a).

4.2. Chemostratigraphic correlation of the Shaler and Mackenzie Mountains supergroups

The Shaler Supergroup has traditionally been correlated with the Mackenzie Mountains Supergroup based on lithostratigraphy (Jefferson and Young, 1977; Rainbird et al., 1996), stromatolite biostratigraphy (Aitken and Long, 1978; Jefferson and Young, 1989), and sequence stratigraphy (Long et al., 2008). The Shaler Supergroup $\delta^{13}C$ records presented here and the high-resolution data from the Mackenzie Mountains (Halverson, 2006) provide a new tool for correlating the rocks in the region. The major assumptions of $\delta^{13}C$ chemostratigraphic correlation schemes are that (a) the $\delta^{13}C$ of the global ocean is well-mixed, such that isotopic trends are recorded worldwide, and (b) the $\delta^{13}C$ values recovered from the rock samples record the $\delta^{13}C$ values of the ocean (or the early diagenetic pore waters) at the time of sedimentation (or earliest diagenesis). Although the Shaler Supergroup was deposited in an intracratonic basin (Rainbird, 1991; Morin and Rainbird, 1993) that may have been intermittently restricted from the open ocean, it would have been connected to the open ocean through cratonic seaways, as fossils recovered from the Wynniatt Formation indicate nonrestricted marine conditions (Butterfield and Rainbird, 1998). Although evaporitic facies occur extensively in the Minto Inlet and Kilian formations, $>$ 95% of the $\delta^{13}C$ data reported here come from non-evaporitic carbonate rocks. The $\delta^{13}C$ secular curve (Fig. 5) is interpreted to represent isotopic trends in the global ocean composition.

With these assumptions, a direct formation-by-formation comparison of the $\delta^{13}C$ records from the Amundsen Basin and the Mackenzie Mountains Supergroup (Fig. 6a) indicates that formations thought to be correlative (Jefferson and Young, 1977; Rainbird et al., 1996) do not host parallel $\delta^{13}C$ curves. The $\delta^{13}C$ profiles do not demonstrate a tight correspondence, and distinctive $\delta^{13}C$ patterns observable in both basins are stratigraphically offset. This observation compels us to consider whether lithostratigraphically equivalent units may have been deposited at different times. Recent work has placed the strata in a sequence stratigraphic framework (Long et al., 2008), loosening the strict formation-by formation correlations and allowing for some temporal variability in time of deposition. Below we outline a hypothesis for the relative timing of the deposits in the Amundsen Basin and Mackenzie Mountains Supergroup that is based on (a) comparison of the $\delta^{13}C$ curves and (b) the assumption that $\delta^{13}C$ trends are isochronous.

An alternate correlation between the two regions can be developed by using distinctive features of the $\delta^{13}C$ curves to drive the correlation (Fig. 6b). This scheme obeys the few geochronological constraints available (see Section 2.2) and attempts to preserve a degree of lithostratigraphic coherence between the two basins. The primary isotopic features used in the correlation are (a) the relatively low $\delta^{13}C$ values of the Aok Formation and the lower Platform Assemblage, (b) the "double positive peaks" in the lower Wynniatt Formation and the lower Upper Carbonate Formation (DPP in Fig. 5), (c) the negative anomalies at the top of the lower Wynniatt Formation and in the middle of the Upper Carbonate Formation, and (d) the negative anomalies in the upper Kilian Formation and the Coates Lake Group. $\delta^{13}C$ data from Katherine Group K6 is not available, making some of the comparisons with the Rae Group less well-constrained. In order to give the best chemostratigraphic correlation to the Mackenzie Mountains Supergroup and to explain the stepwise jump from -5 to $+6$ ‰ within the measured sections of the Wynniatt Formation, a hiatus separating the lower and upper portions of the Wynniatt Formation is introduced. Field evidence for such a hiatus has not yet been observed, but its presence is testable by mapping out the lower-upper Wynniatt Formation contact occupied by a diabase sill at Kilian Lake (near sections S1 and S2), and looking for an exposure where the interval is not intruded by a sill. Measuring the $\delta^{13}C$ of a suite of high-resolution sections through the transition from lower to upper Wynniatt Formation spanning the entire length of the Minto Inlier would strengthen the isotopic record of this key interval.

Studies of Proterozoic, Phanerozoic, and modern oceans show that $\delta^{13}C$ values are spatially variable by as much as 2-3‰ (Hoffman et al., 2007; Kroopnick, 1985; Saltzman et al., 2000; Veizer et al., 1999). For this reason, correlations are generally not based on absolute values, but on parallel secular changes observed in given environments at different locations (e.g., correlation of the Neoproterozoic Tsumeb Subgroup between the Otavi carbonate platform and foreslope in Namibia (Halverson et al., 2005), variable expression of major $\delta^{13}C$ excursions in end Ordovician strata around the globe (Laporte et al., 2009; Melchin and Holmden, 2006; Panchuk et al., 2006), or the compilation of foraminiferal $\delta^{13}C$ data from the Atlantic and Pacific oceans showing clear trends with offset between basins since the middle Miocene (Zachos et al., 2001)).

In Fig. 6, each of the units of the Shaler Supergroup is scaled independently to match either the lithostratigraphy (Fig. 6a) or the chemostratigraphy (Fig. 6b) of the Mackenzie Mountains Supergroup. The graphs on the right side of the Shaler stratigraphic columns show the factor by which each unit was scaled to produce the correlation, based on the measured thicknesses of the Shaler Supergroup and those reported in Halverson (2006) for the Mackenzie Mountains Supergroup. Significant thickness variations have been documented across both basins (Long et al., 2008), and the plots in Fig. 6 would look different if different measured sections were used. The present comparison is made because these are the thicknesses measured for the sections that yielded the $\delta^{13}C$ data under consideration. The lithostratigraphic correlation requires that units scale unevenly. For example, the lower Wynniatt Formation is scaled by a factor of 0.7 while the Boot Inlet Formation is scaled by a factor of 6.5. The mean lithostratigraphic scaling factor is 2.8 ± 2.0. The chemostratigraphic correlation scales each unit more evenly. The mean chemostratigraphic scaling factor is 2.2 ± 0.7. In both cases the Shaler strata are 2–3 times thinner than their counterparts in the Mackenzie Mountains, in agreement with previous measurements (Long et al., 2008). Because the Shaler and Mackenzie Mountains supergroups were probably part of the same subsiding superbasin, we expect a direct relationship between the sediment thicknesses accumulated in each basin over time. This result has potentially interesting implications for the interpretation of basin subsidence mechanisms in the region. In a large restricted basin such as the modern Mediterranean Sea, significant facies changes (due to base level change or uniform subsidence) are recorded as isochronous "bathtub rings." The intracratonic sag model for subsidence in the Amundsen Basin and Mackenzie Mountains may need to be modified to reflect geographically heterogeneous subsidence.

The present chemostratigraphic correlation hypothesis makes predictions about the Coates Lake Group in the Mackenzie Mountains. The Coates Lake Group has been viewed as a physically isolated fault-bounded rift basin without regional or global connections (Jefferson, 1985), and may also be part of Sequence C (Aitken, 1981; Long et al., 2008). The significant $\delta^{13}C$ anomaly it hosts (Halverson, 2006) has not been well integrated into the global Neoproterozoic chemostratigraphic database. However, the data from the upper Kilian Formation exhibit a similar, but less pronounced negative $\delta^{13}C$ anomaly (Fig. 5). The Coates Lake anomaly precedes the Rapitan Group, which includes Sturtian-aged glacial diamictite. The upper Kilian Formation contains a 6–11 m thick purple silty diamictite. One possible interpretation is that the diamictite is a distal equivalent of the glaciogenic Sayunei Formation of the Rapi-

tan Group, the flooding atop the Kilian is related to glacioisostasy or deglacioeustasy, and the limestone ribbonites and breccias are syn- or post-glacial. Although the Kilian and Kuujjua formations contain multiple sedimentary indicators of a hot and arid climate (such as desiccation cracks, halite casts, and tepee structures), the hallmark of Neoproterozoic global glaciation is the sudden appearance of glaciogenic strata worldwide, including on top of tropical carbonate platforms. Even so, the suggestion that the Kilian diamictite is glacial is speculative at this point, as no glaciogenic indicators were observed at the one location where the diamictite was observed (S9). Future field observations and chemostratigraphic work on Victoria Island should be able to determine the lateral extent of the diamictite, its origin, and its association with the negative $\delta^{13}C$ anomaly. Although the negative $\delta^{13}C$ anomaly in the tan carbonate member has been reproduced in the southwest domain (section 05RAT53), it is possible that future work may fail to reproduce the negative anomaly in other outcrops of the upper Kilian Formation, thereby casting doubt upon the validity of the new hypothesis. In the hypothesis presented here, the Kilian and Coates Lake anomalies are correlative and it is suggested that they mark a regional, and potentially global, marine isotopic signal. The possibility of a global negative $\delta^{13}C$ anomaly is considered in Section 4.4.

The BSS is named for the formation where the negative $\delta^{13}C$ anomaly was first thoroughly documented, in Units 1 and 2 of the Loves Creek Member of the Bitter Springs Formation (Amadeus Basin, central Australia), in which $\delta^{13}C$ values change from +5 to −1 and back to +5‰ (Hill et al., 2000; Swanson-Hysell et al., 2008). The anomaly is not associated with glacial deposits, in contrast to many other Neoproterozoic negative $\delta^{13}C$ excursions. Anomalies similar to the Bitter Springs have been reported in correlative strata of the Akademikerbreen Group (northeastern Svalbard) (Halverson et al., 2007b), the Little Dal Group (northwestern Canada), and possibly Ethiopia (Alene et al., 2006). The wide geographic distribution of these sections in current reconstructions of Rodinia (Li et al., 2008) suggests that the anomaly is representative of the $\delta^{13}C$ of the global ocean.

The other possible correlation of the upper Kilian anomaly is with the globally documented "Bitter Springs Stage" (BSS) negative anomaly (Halverson et al., 2005, 2007b; Maloof et al., 2006) in the Upper Carbonate Formation. The BSS is named for the formation where the negative $\delta^{13}C$ anomaly was first thoroughly documented, in Units 1 and 2 of the Loves Creek Member of the Bitter Springs Formation (Amadeus Basin, central Australia), in which $\delta^{13}C$ values change from +5 to −1 and back to +5‰ (Hill et al., 2000; Swanson-Hysell et al., 2008). The anomaly is not associated with glacial deposits, in contrast to many other Neoproterozoic negative $\delta^{13}C$ excursions. Anomalies similar to the Bitter Springs have been reported in correlative strata of the Akademikerbreen Group (northeastern Svalbard) (Halverson et al., 2007b), the Little Dal Group (northwestern Canada), and possibly Ethiopia (Alene et al., 2006). The wide geographic distribution of these sections in current reconstructions of Rodinia (Li et al., 2008) suggests that the anomaly is representative of the $\delta^{13}C$ of the global ocean. Correlation of the upper Kilian Formation $\delta^{13}C$ anomaly with the BSS many difficult implications. First, it eliminates the tight correspondence of the "double positive peaks" in the $\delta^{13}C$ stratigraphy (DPP on Fig. 5). Second, it either (a) negates all the lithostratigraphic correlations between the formations below the Wynniatt and Upper Carbonate formations, or (b) requires a tremendous increase in sedimentation accumulation rate beginning at the base of the Wynniatt and continuing through the rest of the Shaler Supergroup. While such a subsidence history might be expected in a foreland or active rift basin, the Shaler stratigraphy and regional geology are inconsistent with such an active tectonic setting. Third, correlation of the upper Kilian and "Bitter Springs" anomalies would require a long hiatus (>80 Ma) between the allegedly Bitter Springs-aged Kuujjua Formation and the Natkusiak basalts. However, Rainbird (1993) has demonstrated that the Kuujjua Formation was unlithified at the time of the Natkusiak eruptions. For these reasons a "Bitter Springs Stage" age for the Kilian Formation is unlikely.

The new $\delta^{13}C$ correlation hypothesis suggests that many of the units in the Rae Group may not have been deposited at the same time as their proposed lithostratigraphic equivalents in the Mackenzie Mountains Supergroup. The distinctive orange-weathering stromatolitic dolostones of the Aok Formation have frequently been used as a regional marker bed assumed to be correlative with the K6 Formation of the Katherine Group in the Mackenzie Mountains (Jefferson and Young, 1989). This correlation implies an exceptionally extensive stromatolitic buildup contemporaneously spanning the Amundsen Basin and the Mackenzie Mountains region. The new $\delta^{13}C$ -based correlation suggests that the Aok may instead be temporally correlative with the lower Platform Assemblage of the Little Dal Group. Further $\delta^{13}C$ work on the Rae and Little Dal groups will help to elucidate temporal variability between lithostratigraphically equivalent units, as the chemostratigraphic correlation presented here implies that few of the lithostratigraphic correlatives are exactly chronostratigraphically equivalent. Rather, the $\delta^{13}C$ correlation hypothesis suggests that facies patterns migrated over time between the Mackenzie and Amundsen Embayments in response to relatively higher subsidence rates in the Mackenzie Mountains basin.

The sequence architecture inferred from the $\delta^{13}C$ correlation is most evident in the lower part of the stratigraphy (Fig. 6). Under the new hypothesis, the stromatolites of Katherine Group K6 and the sandstones of Katherine Group K7 are older than their lithological equivalents in the Shaler Supergroup, the Aok and Grassy Bay formations. If this is the case, these facies must have prograded from the Mackenzie Mountains basin to the Amundsen Basin. Based on detrital zircon geochronology and provenance studies, Rainbird et al. (1997) proposed that the Katherine Group and Nelson Head Formation are remnants of an extensive and long-lived fluvial sand sheet sedimentary system originating from the Grenville orogen.

Similarly, the chemostratigraphic correlation hypothesis predicts that carbonate sedimentation resumed diachronously after the sandstones were laid down, first in the Mackenzie Mountains and then in the Amundsen Basin; the Mudcracked Formation and lower Platform Assemblage are older than the lower Boot Inlet Formation. This suggests that facies were still prograding from the Mackenzie Mountains to the Amundsen Basin. However, the carbon isotope correlation indicates that by the end of Platform Assemblage/Boot Inlet time both basins were depositing similar facies contemporaneously. From this point on neither basin significantly leads or lags in their depositional environment. Such a history is expected if non-uniform lithospheric stretching were responsible for the origin of the intracratonic sag; initial thinning would cause varying subsidence rates in the region, but once thinning ended thermal subsidence would cause the entire region to subside uniformly.

The new correlation hypothesis presented here is generally consistent with the earlier correlations (Jefferson and Young, 1977; Aitken and Long, 1978; Rainbird et al., 1996) but also introduces several points of variance for further study and testing. A more detailed picture of shifting facies patterns in northwest Laurentia in the Neoproterozoic may result from this approach. The data also suggest a new hypothesis regarding the source of accommodation space in the basin: lithospheric thinning caused inhomogeneous intracratonic sag until Platform Assemblage/Boot Inlet Formation time, at which point thermal subsidence produced uniform subsidence across the region.

4.3. The "Bitter Springs" anomaly and TPW

The "Bitter Springs Stage" (BSS) negative $\delta^{13}C$ anomaly has been documented in multiple Neoproterozoic basins throughout the world (e.g., Halverson et al., 2005, 2007b; Alene et al., 2006; Hill et al., 2000; Maloof et al., 2006). Its absence in the Shaler Supergroup is a potentially problematic result of the hypothesis proposed here (Fig. 6). If the proposed correlation is correct then the data presented here lead to two possible interpretations: (a) the Amundsen Basin did not always record the $\delta^{13}C$ of the global ocean, or (b) there is a disconformity due to ~10 to 15 Ma of missing stratigraphy. Each of these possibilities is considered in turn.

During times of evaporite deposition, the Amundsen Basin likely was not in complete chemical exchange with the global ocean. Carbonates interbedded with gypsum and anhydrite in the Minto Inlet Formation record $\delta^{13}C$ values of ~ -1 ‰, which is significantly depleted from the +5 ‰ values of carbonates bracketing the evaporite units. Similar isotopic depletion has been observed in evaporites of the Gillen Member of the Bitter Springs Formation (N. Swanson-Hysell, personal communication). However, these indicators of basin restriction are not constant throughout the Shaler Supergroup, which is dominated by peritidal and shallow marine carbonate deposits. Additionally, the bulk of the Shaler $\delta^{13}C$ record correlates very well with the $\delta^{13}C$ of the Mackenzie Mountains, the Amadeus Basin, and the Akademikerbreen Group. The simplest explanation for the concordance of the $\delta^{13}C$ stratigraphy of these sequences is that they are all recording the same changes to the global carbon cycle.

Could a profound disconformity separate the lower and upper Wynniatt Formation? Although such a disconformity has not yet been observed in the field, several lines of reasoning suggest that it is possible. The first consideration is the duration of the basin subsidence, which is a question that has little firm geochronological control. However, if the basin began to subside (e.g., intracratonic sag due to lithospheric thinning) sometime after 1077 Ma (the maximum age of the Nelson Head Formation of the Rae Group based on detrital zircon geochronology (Rainbird et al., 1997)), thermal models of basin evolution would suggest that the development of new accommodation space would taper off within the next 150 million years (McKenzie, 1978). That is significantly earlier than 812 Ma, which is the best estimate of the age of the initiation of the BSS, based on U–Pb dating of zircons from the Fifteenmile Group in the central Ogilvie Mountains near the Alaska-Yukon border (Macdonald et al., 2010).

The BSS has been attributed to a pair of true polar wander (TPW) events in the middle Neoproterozoic (Maloof et al., 2006). Two independent data sets suggest that the TPW rotation pole pierced equatorial Laurentia (Li et al., 2004; Maloof et al., 2006) . Because this pole is inferred to have been close to the location of the Amundsen Basin, a TPW rotation about this axis would not have forced a rapid shift in the Amundsen Basin's paleolatitude. Therefore, any attendant changes in relative sea level due to reconfiguration of the equatorial bulge would have been minimal at the Amundsen Basin, and possibly not observable in the geologic record (Mound and Mitrovica, 1998; Mound et al., 1999). Furthermore, the region would have stayed in the warm tropical belt of carbonate precipitation, so no marked change in lithology would correspond to the onset of a TPW event.

4.4. The pre-Sturtian "Islay Excursion"

The upper tie point of the Amundsen-Mackenzie chemostratigraphic correlation hypothesis proposed here is pinned to the architecture (although not the absolute values) of the negative $\delta^{13}C$ excursions measured in the Kilian Formation and Coates Lake Group (Fig. 6). The Kilian and Coates Lake excursions are reminiscent of negative $\delta^{13}C$ anomalies underneath older Cryogenian glacial deposits. In East Greenland, bed-groups 19 and 20 of the uppermost part of the Eleanore Bay Supergroup host a negative anomaly beneath the glaciogenic UlvesøFormation of the overlying Tillite Group (Fairchild et al., 2000). In the Togari Group of northwest Tasmania it is the Black River Dolomite that hosts a negative excursion below glacial diamictite of the Julius River Member (Calver, 1998). In the Dalradian Supergroup of Scotland, the Lossit or Islay Limestone contains an anomaly below the Port Askaig Tillite of the Argyll Group (Brasier and Shields, 2000; McCay et al., 2006). In northeast Svalbard, the RussoyøMember of the Elbobreen Formation has a well-documented negative $\delta^{13}C$ excursion beneath the Petrovbreen diamictite, which was originally interpreted as an older Cryogenian glacial deposit (Brasier and Shields, 2000), reinterpreted as younger Cryogenian (Halverson et al., 2004), before reaffirmation as an older Cryogenian deposit on the basis of new Sr-isotope data (Halverson et al., 2007a).

The Kilian Formation, which underlies the Natkusiak basalts, is constrained to be older than 723 Ma because it is intruded by diabase sills of this age (Heaman et al. (1992) and Section 2.2). The Coates Lake Group sits unconformably on the Little Dal basalt. Although it has not been confirmed geochronologically, the Little Dal basalt may be cogenetic with 779 Ma dikes and sills in the northern Cordillera (LeCheminant and Heaman, 1994); these dikes and sills intrude the Little Dal and Katherine groups, but not the overlying Coates Lake Group (Jefferson and Parrish, 1989). If the Kilian and Coates Lake excursions are correlative, they should therefore fall between 779 and 723 Ma.

The negative carbon isotope anomaly found in the Kilian Formation below a 6–11 m thick purple silty diamictite at S9 (see Section 2.1) may be correlative with the anomalies found below older Cryogenian ("Sturtian") glacial deposits worldwide. It is here referred to as the "Islay Excursion" after the location where it was first documented (Brasier and Shields, 2000). The existence of a negative carbon isotope anomaly before the older Cryogenian glaciation is analogous to the well-documented Trezona anomaly found below younger Cryogenian ("Marinoan") glacial deposits (as reviewed in Halverson et al. (2005); Halverson (2006)). As more data becomes available it may become apparent that the global carbon cycle instability represented by these negative carbon isotope excursions occurred before the older Cryogenian snowball glaciations as well as the younger Marinoan glaciation. On Victoria Island, the putative glacial diamictite observed at section S9 of the upper Kilian Formation needs to be studied in more detail to confirm glacial features and needs to be located elsewhere in the basin. If it can be shown to be laterally extensive, and if the carbonates associated with it do indeed have depleted $\delta^{13}C$ values, then the Shaler Supergroup would lend support to a pre-Sturtian negative anomaly. However, negative anomalies of similar magnitude that are not associated with glaciation have been documented in the mid-Cryogenian (Macdonald et al., 2009a) and possibly mid-Ediacaran (Calver, 2000; Fike et al., 2006; McFadden et al., 2008). The origins of these negative anomalies and their relation to climate catastrophe and reorganization of geochemical cycles remain as unresolved questions in Neoproterozoic Earth history.

4.5. Global correlation

The $\delta^{13}C$ correlation hypothesis presented here allows the geochemical and paleontological records of the Shaler Supergroup to be integrated into the history of the Neoproterozoic Earth. The $\delta^{13}C$ record from the Shaler Supergroup shows good agreement with features of the global composite $\delta^{13}C$ curve (Fig. 7) (Halverson et al., 2007a), including the following: (a) a rising trend in the early

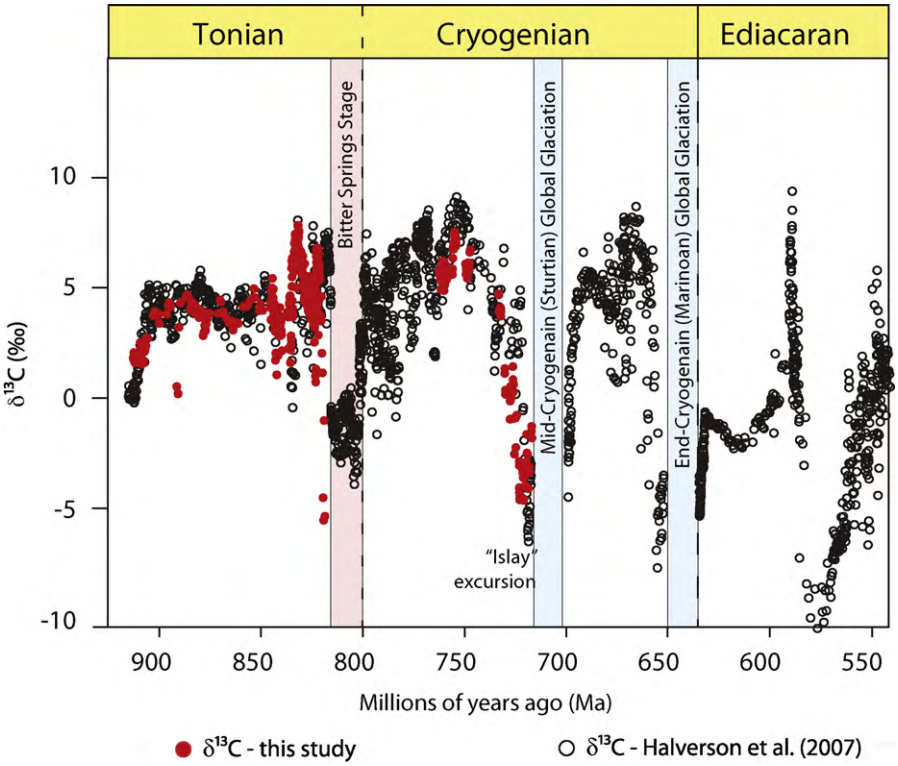

Fig. 7. Integration of the $\delta^{13}C$ data presented here with the global composite record, modified from Halverson et al. (2007a). The base of the Cryogenian is undefined, and is placed here coincident with the end of the "Bitter Springs Stage" (Halverson et al., 2008).

Tonian period leading to an interval of relatively constant $\delta^{13}C$ values centered around ~4 ‰; (b) the double positive peaks that rise up to ~8 ‰ preceding the Bitter Sprints isotopic stage; (c) an early Cryogenian peak followed by a well-defined negative $\delta^{13}C$ excursion ("Islay excursion") prior to the "Sturtian" global glaciation. The suggested duration of subsidence (~180 Ma, Fig. 7) and thickness of sediment accumulated (> 1 km, Fig. 5) are consistent with geophysical models of long-term subsidence of intracratonic basins (Armitage and Allen, 2010).

The Shaler Supergroup has yielded a small but significant amount of early Neoproterozoic paleontological data. A diverse suite of acritarchs (Butterfield and Rainbird, 1998) and carbonaceous megafossils of the *Chuaria-Tawuia* assemblage (Hofmann and Rainbird, 1995) have been described from the lower Wynniatt Formation. A complex eukaryote (Butterfield, 2005a) and dinoflagellates (Butterfield and Rainbird, 1998) have been identified in these strata. If the chemostratigraphic correlation hypothesis is confirmed, the lower Wynniatt Formation, and therefore the biota it hosts, directly predates the BSS. This is a new constraint on the relative timing isotopic events and biological evolution in the Neoproterozoic.

5. Conclusions

New high-resolution carbon isotope data from the Shaler Supergroup of Arctic Canada provide an expanded view of geochemical fluctuations during the early Neoproterozoic. This study uses detailed $\delta^{13}C$ data from the Shaler Supergroup to develop a new, testable hypothesis for correlation with the Mackenzie Mountains Supergroup. Using secular variations $\delta^{13}C$ as an independent chronometer, the new hypothesis is based on matching distinctive features of the $\delta^{13}C$ curves from both basins. Doing so reveals that lithologically correlative units were deposited diachronously; depositional environments migrated from one basin to the other over time. A consequence of the new correlation scheme is that the biota hosted in the Wynniatt Formation of the Shaler Supergroup was deposited prior to the globally observed "Bitter Springs" isotopic stage. This provides a new means of integrating the paleobiological data into the global record of Neoproterozoic Earth history.

Acknowledgments

Dave Maloley and Polar Continental Shelf Project (PCSP) provided logistical support in the field. Funding was provided by a PCSP grant to Maloof and a National Science Foundation Graduate Research Fellowship to Jones. Paul Hoffman, Andy Knoll, and Francis Macdonald provided insightful comments on an earlier draft of this paper. Greg Eischeid guided the preparation of samples for isotopic analysis. Two anonymous reviewers are thanked for their constructive feedback.

References

Aitken, J.D., Long, D.G.F., 1978. Correlation of Helikian strata, Mackenzie Mountains - Brock Inlier - Victoria Island. Geological Survey of Canada Current Research 1A, 485–486.

Aitken, J.D., 1981. Stratigraphy and sedimentology of the upper Proterozoic Little Dal Group, Mackenzie Mountains, Northwest Territories. Geological Survey of Canada Paper 81–10, 47–71.

Alene, M., Jenkin, G., Leng, M., Darbyshire, D., 2006. The Tambien Group, Ethiopia: an early Cryogenian (ca. 800–735 Ma) Neoproterozoic sequence in the Arabian–Nubian Shield. Precambrian Research 147, 79–99.

Allen, P.A., Hoffman, P.F., 2005. Extreme winds and waves in the aftermath of a Neoproterozoic glaciation. Nature 433, 123–127.

Anbar, A.D., Knoll, A.H., 2002. Proterozoic ocean chemistry and evolution: a bioinorganic bridge? Science 297, 1137–1142.

Armitage, J.J., Allen, P.A., 2010. Cratonic basins and the long-term subsidence history of continental interiors. Journal of the Geological Society London 167, 61–70.

Asmerom, Y., Jacobsen, S., Knoll, A.H., Butterfield, N., Swett, K., 1991. Strontium isotopic variations of Neoproterozoic seawater: implications for crustal evolution. Geochimica et Cosmochimica Acta 55, 2883–2894.

Baragar, W.R.A., Donaldson, J.A., 1973. Coppermine and Dismal Lakes map areas. Geological Survey of Canada Paper 71–39, 20.
Bartley, J.K., Kah, L.C., 2004. Marine carbon reservoir, Corg-Ccarb coupling, and the evolution of the Proterozoic carbon cycle. Geology 32, 129–133.
Boulvais, P., Fourcade, S., Gruau, G., Moine, B., 1998. Persistence of pre-metamorphic C and O isotopic signatures in marbles subject to Pan-African granulite-facies metamorphism and U–Th mineralization (Tranomaro, Southeast Madagascar). Chemical Geology 150, 247–262.
Brasier, M., Shields, G., 2000. Neoproterozoic chemostratigraphy and correlation of the Port Askaig glaciation, Dalradian Supergroup of Scotland. Journal of the Geological Society London 157, 909–914.
Butterfield, N., Rainbird, R.H., 1998. Diverse organic-walled fossils, including possible dinoflagellates, from the early Neoproterozoic of arctic Canada. Geology 26, 963–966.
Butterfield, N., 2005a. Reconstructing a complex early Neoproterozoic eukaryote, Wynniatt Formation, arctic Canada. Lethaia 38, 155–169.
Butterfield, N., 2005b. Probable Proterozoic fungi. Paleobiology 31, 165–182.
Calver, C.R., 1998. Isotope stratigraphy of the Neoproterozoic Togari Group, Tasmania. Australian Journal of Earth Sciences 45, 865–874.
Calver, C.R., 2000. Isotope stratigraphy of the Ediacarian (Neoproterozoic III) of the Adelaide Rift Complex, Australia, and the overprint of water column stratification. Precambrian Research 100, 121–150.
Campbell, F.H.A., 1981. Stratigraphy and tectono-depositional relationships of the Proterozoic rocks of the Hadley Bay area, northern Victoria Island, District of Franklin. Current Research, Part A, Geological Survey of Canada Paper 81-1A, 15–22.
Christie, R.L., Fyles, J.G., Thorsteinsson, R., Tozer, E.T., 1963. Geology of Banks, Victoria and Stefansson Islands, District of Franklin. "A" Series Map. Geological Survey of Canada.
Derry, L.A., Kaufman, A.J., Jacobsen, S.B., 1992. Sedimentary cycling and environmental change in the Late Proterozoic-Evidence from stable and radiogenic isotopes. Geochimica et Cosmochimica Acta, 1317–1329.
Dostal, J., Barager, W.R.A., Dupuy, C., 1986. Petrogenesis of the Natkusiak continental basalts, Victoria Island, Northwest Territories, Canada. Canadian Journal of Earth Science 23, 622–632.
Fairchild, I., Spiro, B., Herrington, P.M., Song, T., 2000. Controls on Sr and C isotope compositions of Neoproterozoic Sr-rich limestones of East Greenland and North China. In: Grotzinger, J.P., James, N.P. (Eds.), Carbonate Sedimentation and Diagenesis in the Evolving Precambrian World. Number 67 in SEPM Special Publications, SEPM (Society for Sedimentary Geology), pp. 297–313.
Fike, D.A., Grotzinger, J.P., Pratt, L.M., Summons, R.E., 2006. Oxidation of the Ediacaran ocean. Nature 444, 744–747.
Halverson, G.P., Maloof, A.C., Hoffman, P.F., 2004. The Marinoan glaciation (Neoproterozoic) in northeast Svalbard. Basin Research 16, 297–324.
Halverson, G.P., Hoffman, P.F., Schrag, D.P., Maloof, A.C., Rice, A.H.N., 2005. Toward a Neoproterozoic composite carbon-isotope record. Geological Society America Bulletin 117, 1181–1207.
Halverson, G.P., Dudas, F.O., Maloof, A.C., Bowring, S.A., 2007a. Evolution of the 87Sr/86Sr composition of Neoproterozoic seawater. Palaeogeography Palaeoclimatology Palaeoecology 256, 103–129.
Halverson, G.P., Maloof, A.C., Schrag, D.P., Dudas, F.O., Hurtgen, M., 2007b. Stratigraphy and geochemistry of a ca 800 Ma negative carbon isotope interval in northeastern Svalbard. Chemical Geology 237, 5–27.
Halverson, G.P., Maloof, A.C., Hurtgen, M.T., 2008. The Cryogenian section in northeastern Svalbard. In: International Geological Congress.
Halverson, G.P., 2006. A Neoproterozoic chronology. In: Xiao, S., Kaufman, A.J. (Eds.), Neoproterozoic Geobiology and Paleobiology, volume 27 of Topics in Geobiology. chapter 8, Springer, pp. 231–271.
Heaman, L., LeCheminant, A.N., Rainbird, R.H., 1992. Nature and timing of Franklin igneous events, Canada: implications for a late Proterozoic mantle plume and the break-up of Laurentia. Earth and Planetary Science Letters 109, 117–131.
Hill, A., Walter, M., 2000. Mid-Neoproterozoic (830–750 Ma) isotope stratigraphy of Australia and global correlation. Precambrian Research 100 (1), 181–211.
Hill, A., Arouri, K., Gorjan, P., Walter, M., 2000. Geochemistry of marine and nonmarine environments of a Neoproterozoic cratonic carbonate/evaporite: the Bitter Springs Formation, central Australia. In: Grotzinger, J.P., James, N.P. (Eds.), Carbonate Sedimentation and Diagenesis in the Evolving Precambrian world. Number 67 in SEPM Special Publications, SEPM (Society for Sedimentary Geology), pp. 327–344.
Hoffman, P.F., Halverson, G.P., Domack, E.W., Husson, J., Higgins, J.A., Schrag, D.P., 2007. Are basal Ediacaran (635 Ma) post-glacial cap dolostones diachronous? Earth and Planetary Science Letters 258, 114–131.
Hoffman, P.F., 1999. The break-up of Rodinia, birth of Gondwana, true polar wander and the snowball Earth. Journal of African Earth Sciences 28, 17–33.
Hofmann, H., Rainbird, R.H., 1995. Carbonaceous megafossils from the Neoproterozoic Shaler Supergroup of Arctic Canada. Palaeontology 37, 721–731.
Jefferson, C.W., Parrish, R.R., 1989. Late Proterozoic stratigraphy, U–Pb zircon ages, and rift tectonics Mackenzie Mountains. Canadian Journal of Earth Sciences 26, 1784–1801.
Jefferson, C.W., Young, G.M., 1977. Use of stromatolites in regional lithological correlations of Upper Proterozoic successions of the Amundsen Basin and Mackenzie Mountains Canada. Geological Association of Canada Program with Abstracts 2, 26.
Jefferson, C.W., Young, G.M., 1989. Late Proterozoic orange-weathering stromatolite biostrome Mackenzie Mountains and western Arctic Canada. Canadian Society of Petroleum Geologists Memoir 13, 72–80.
Jefferson, C.W., 1985. Uppermost Shaler Group and its contact with the Natkusiak basalts, Victoria Island District of Franklin. Geological Survey of Canada Current Research 85-1A, 103–110.
Kaufman, A.J., Knoll, A.H., 1995. Neoproterozoic variations in the C-isotopic composition of seawater: stratigraphic and biogeochemical implications. Precambrian Research 73, 27–49.
Kaufman, A.J., Hayes, J.M., Knoll, A.H., Germs, G.J.B., 1991. Isotopic compositions of carbonates and organic carbon from upper Proterozoic successions in Namibia: stratigraphic variation and the effects of diagenesis and metamorphism. Precambrian Research 49, 301–327.
Kroopnick, P.M., 1985. The distribution of $\delta^{13}C$ of ΣCO_2 in the world oceans. Deep-Sea Research 32, 57–84.
Laporte, D.F., Holmden, C.E., Patterson, W.P., Loxton, J.D., Melchin, M.J., Mitchell, C.E., Finney, S.C., Sheets, H.D., 2009. Local and global perspectives on carbon and nitrogen cycling during the Hirnantian glaciation. Palaeogeography Palaeoclimatology Palaeoecology 276 (1–4), 182–195.
LeCheminant, A.N., Heaman, L., 1989. Mackenzie igneous events, Canada: middle Proterozoic hotspot magmatism associated with ocean opening. Earth and Planetary Science Letters 96, 38–48.
LeCheminant, A., Heaman, L., 1994. 779 Ma mafic magmatism in the northwestern Canadian Shield and northern Cordillera: a new regional time-marker. In: Proceedings of the 8th International Conference on Geochronology, Cosmochronology and Isotope Geology, vol. 1107, p. 197.
Li, Z.X., Evans, D., Zhang, S., 2004. A 90° spin on Rodinia: possible causal links between the Neoproterozoic supercontinent, superplume, true polar wander and low-latitude glaciation. Earth and Planetary Science Letters 220, 409–421.
Li, Z.X., Bogdanova, S.V., Collins, A.S., Davidson, A., Waele, B.D., Ernst, R.E., Fitzsimons, I.C.W., Fuck, R.A., Gladkochub, D.P., Jacobs, J., Karlstrom, K.E., Lu, S., Natapov, L.M., Pease, V., Pisarevsky, S.A., Thrane, K., Vernikovsky, V., 2008. Assembly, configuration, and break-up history of Rodinia: a synthesis. Precambrian Research 160, 179–210.
Long, D.G.F., Rainbird, R.H., MacNaughton, R.B., 2008. Early Neoproterozoic strata (Sequence B) of mainland northern Canada and Victoria and Banks islands. Open File Report 5700, Geological Survey of Canada.
Macdonald, F.A., Jones, D.S., Schrag, D.P., 2009a. Stratigraphic and tectonic implications of a newly discovered glacial diamictite-cap carbonate couplet in southwestern Mongolia. Geology 37, 123–126.
Macdonald, F.A., McClelland, W.C., Schrag, D.P., Macdonald, W.P., 2009b. Neoproterozoic glaciation on a carbonate platform margin in Arctic Alaska and the origin of the North Slope suberrane. Geological Society of America Bulletin 121, 448–473.
Macdonald, F.A., Schmitz, M.D., Crowley, J.L., Roots, C.F., Jones, D.S., Maloof, A.C., Strauss, J.V., Cohen, P.A., Johnston, D.T., Schrag, D.P., 2010. Calibrating the Cryogenian. Science 327, 1241–1243.
Maloof, A.C., Halverson, G.P., Kirschvink, J.L., Schrag, D.P., Weiss, B.P., Hoffman, P.F., 2006. Combined paleomagnetic, isotopic, and stratigraphic evidence for true polar wander from the Neoproterozoic Akademikerbreen Group, Svalbard, Norway. Geological Society of America Bulletin 118, 1099–1124.
McCay, G., Prave, A., Alsop, G., Fallick, A., 2006. Glacial trinity: Neoproterozoic Earth history within the British–Irish Caledonides. Geology 34, 909–912.
McFadden, K., Huang, J., Chu, X., Jiang, G., Kaufman, A., 2008. Pulsed oxidation and biological evolution in the Ediacaran Doushantuo Formation. Proceedings of the National Academy of Sciences.
McKenzie, D., 1978. Some remarks on the development of sedimentary basins. Earth and Planetary Science Letters 40, 25–32.
Melchin, M.J., Holmden, C.E., 2006. Carbon isotope chemostratigraphy in Arctic Canada: sea-level forcing of carbonate platform weathering and implications for Hirnantian global correlation. Palaeogeography Palaeoclimatology Palaeoecology 234, 186–200.
Morin, J., Rainbird, R.H., 1993. Sedimentology and sequence stratigraphy of the Neoproterozoic Reynolds Point Formation, Minto Inlier, Victoria Island, Northwest Territories. Geological Survey of Canada Survey Current Research, Part C 93-1C, 7–18.
Mound, J.E., Mitrovica, J.X., 1998. True polar wander as a mechanism for second-order sea-level variations. Science 279, 534–537.
Mound, J.E., Mitrovica, J.X., Evans, D.A.D., Kirschvink, J.L., 1999. A sea-level test for inertial interchange true polar wander events. Geophysical Journal International 136, F5–F10.
Narbonne, G.M., James, N.P., Rainbird, R.H., Morin, J., 2000. Early Neoproterozoic (Tonian) patch reef complexes, Victoria Island, arctic Canada. In: Grotzinger, J.P., James, N.P. (Eds.), Carbonate Sedimentation and Diagenesis in the Evolving Precambrian World. Number 67 in SEPM Special Publications, SEPM (Society for Sedimentary Geology), pp. 163–177.
Panchuk, K., Holmden, C.E., Leslie, S., 2006. Local controls on carbon cycling in the ordovician midcontinent region of north America, with implications for carbon isotope secular curves. Journal of Sedimentary Research 76 (2), 200–211.
Rainbird, R.H., Heaman, L., Young, G.M., 1992. Sampling Laurentia: detrital zircon geochronology offers evidence for an extensive Neoproterozoic river system originating from the Grenville orogen. Geology 20, 351–354.
Rainbird, R.H., Jefferson, C.W., Hildebrand, R.S., Worth, J.K., 1994. The Shaler Supergroup and revision of Neoproterozoic stratigraphy in Amundsen Basin, Northwest Territories. Geological Survey of Canada Current Research C, 61–70.
Rainbird, R.H., Hodgson, D.A., Jefferson, C.W., 1995. Bedrock and surficial geology, Kilian Lake (NTS 78 B/4), District of Franklin, Northwest Territories. Technical report, Geological Survey of Canada Open File.

Rainbird, R.H., Jefferson, C.W., Young, G.M., 1996. The early Neoproterozoic sedimentary succession B of northwestern Laurentia: correlations and paleogeographic significance. Geological Society of America Bulletin 108, 454–470.
Rainbird, R.H., McNicoll, V., Theriault, R., 1997. Pan-continental river system draining greenville orogen recorded by U–Pb and Sm–Nd geochronology of Neoproterozoic quartzarenites and mudrocks northwestern Canada. The Journal of Geology.
Rainbird, R.H., 1991. Stratigraphy, Sedimentology and Tectonic Setting of the Upper Shaler Group, Victoria Island, Northwest Territories. PhD Thesis, University of Western Ontario.
Rainbird, R.H., 1993. The sedimentary record of mantle plume uplift preceding eruption of the Neoproterozoic Natkusiak flood basalt. The Journal of Geology 101 (3), 305–318.
Saltzman, M., Ripperdan, R., Brasier, M., Lohmann, K., Robison, R., Chang, W., Peng, S., Ergaliev, E., Runnegar, B., 2000. A global carbon isotope excursion (SPICE) during the Late Cambrian: relation to trilobite extinctions, organic-matter burial and sea level. Palaeogeography Palaeoclimatology Palaeoecology 162, 211–223.
Shieh, Y., Taylor, H., 1969. Oxygen and carbon isotope studies of contact metamorphism of carbonate rocks. Journal of Petrology 10, 307–331.
Swanson-Hysell, N.L., Maloof, A.C., Halverson, G.P., Hurtgen, M.T., 2008. Covariation in the carbon isotopes of carbonate and organic carbon across the Neoproterozoic Bitter Springs Stage. In: AGU Fall Meeting Abstracts, December, 2008, pp. B1414+.
Thorkelson, D.J., Abbott, J.G., Mortensen, J.K., Creaser, R.A., Villeneuve, M.E., McNicoll, V.J., Layer, P.W., 2005. Early and middle Proterozoic evolution of Yukon Canada. Canadian Journal of Earth Sciences 42, 1045–1071.
Thorsteinsson, R., Tozer, E.T., 1962. Banks, Victoria, and Stefansson Islands, Arctic Archipelago. Geological Survey of Canada Memoir, 330.
Veizer, J., Ala, D., Azmy, K., Bruckschen, P., Buhl, D., Bruhn, F., Carden, G.A.F., Diener, A., Ebneth, S., Godderis, Y., Jasper, T., Korte, C., Pawellek, F., Podlaha, O., Strauss, H., 1999. $^{87}Sr/^{86}Sr$, $\delta^{13}C$ and δ^{18} O evolution of Phanerozoic seawater. Chemical Geology 161, 59–88.
Young, G.M., Long, D.G.F., 1977. A tide-influenced delta complex in the upper Proterozoic Shaler Group Victoria Island Canada. Canadian Journal of Earth Sciences 14, 2246–2261.
Young, G.M., Jefferson, C.W., Delaney, G., Yeo, G., 1979. Middle and late Proterozoic evolution of the northern Canadian Cordillera and Shield. Geology 7, 125–128.
Young, G.M., 1981. The Amundsen Embayment, Northwest Territories; relevance to the upper Proterozoic evolution of North America. Geological Survey of Canada Paper 81, 203–218.
Zachos, J.C., Pagani, M., Sloan, L., Thomas, E., Billups, K., 2001. Trends, rhythms, and aberrations in global climate 65 Ma to present. Science 292, 686–693.